The *Staphylococcus aureus* non-coding RNA IsrR regulates TCA cycle activity and virulence.

Gustavo Rios-Delgado[1], Aubrey K. G. McReynolds[5], Emma A. Pagella[5], Javiera Norambuena[1], Paul Briaud[7], Vincent Zheng[1], Matthew J. Munneke[4], Jisun Kim[3], Hugo Racine[2], Ronan Carroll[7], Ehud Zelzion[6], Eric Skaar[4], Jeffrey L. Bose[5], Dane Parker[3], David Lalaouna[2], Jeffrey M. Boyd[1]

[1] Department of Biochemistry and Microbiology, Rutgers, the State University of New Jersey, New Brunswick, NJ, 08901, USA.
[2] Université de Strasbourg, CNRS, Architecture et Réactivité de l'ARN, UPR9002, Strasbourg, 67000, France
[3] Department of Pathology, Immunology and Laboratory Medicine, Center for Immunity and Inflammation, Rutgers New Jersey Medical School, Newark, New Jersey, 07103, USA.
[4] Department of Pathology, Microbiology, and Immunology, Vanderbilt University Medical Center, Nashville, TN, 37232, USA.
[5] Department of Microbiology, Molecular Genetics, and Immunology, University of Kansas Medical Center, Kanas City, KS, 66103, USA
[6] Office of Advanced Research Computing, Rutgers University, 96 Frelinghuysen Road Piscataway, NJ 08854, USA
[7] Department of Biological Sciences, Ohio University, Athens, OH, 45701, USA

*To whom correspondence may be addressed:
Jeffrey M. Boyd, Department of Biochemistry and Microbiology, Rutgers University, 76 Lipman Drive, New Brunswick, New Jersey, 08901, Telephone: (848) 932-5604, E-mail: jeffboyd@SEBS.rutgers.edu.

Running Title: IsrR regulates TCA cycle.

Keywords: iron, Fur, *Staphylococcus aureus*, Tsr25, IsrR

Abstract

Staphylococcus aureus has evolved mechanisms to cope with low iron (Fe) availability in host tissues. *S. aureus* uses the ferric uptake transcriptional regulator (Fur) to sense titers of cytosolic Fe. Upon Fe depletion, apo-Fur relieves transcriptional repression of genes utilized for Fe uptake. We demonstrate that an *S. aureus* Δ*fur* mutant has decreased expression of *acnA*, which codes for the Fe-dependent enzyme aconitase. This prevents the Δ*fur* mutant from growing with amino acids as sole carbon and energy sources. We used a suppressor screen to exploit this phenotype and determined that a mutation that decreases the transcription of *isrR*, which produces a regulatory RNA, increased *acnA* expression, thereby enabling growth. Directed mutation of bases predicted to facilitate the interaction between the *acnA* transcript and IsrR, decreased the ability of IsrR to control *acnA* expression *in vivo* and IsrR bound to the *acnA* transcript *in vitro*. IsrR also bound transcripts coding the alternate TCA cycle proteins *sdhC*, *mqo*, *citZ*, and *citM*. Whole-cell metal analyses suggest that IsrR promotes Fe uptake and increases intracellular Fe not ligated by macromolecules. Lastly, we determined that Fur and IsrR promote infection using murine skin and acute pneumonia models.

Introduction

Staphylococcus aureus is an infectious agent and a primary cause of morbidity and mortality worldwide. It is commonly associated with community- and hospital-acquired infections, and it can cause a variety of ailments, from minor soft tissue infections to more severe diseases, including septicemia and endocarditis (1). A subset of *S. aureus* associated infections are caused by strains resistant to commonly prescribed antibiotics, complicating treatment (2).

The acquisition of ionic iron (Fe) is essential for *S. aureus*. *S. aureus* strains defective in the acquisition, uptake, or proper usage of intracellular Fe have decreased virulence in models of infection (3-6). The importance of Fe is highlighted by the fact that approximately 2% of the genomic protein-coding open reading frames (ORFs) code for Fe acquisition systems. Iron functions as a cofactor to many proteins, including iron-sulfur (Fe-S) cluster enzymes utilized for respiration and the tricarboxylic acid (TCA) cycle (7).

One strategy that mammals use to combat infections is to limit the availability of nutrients that are essential for bacterial growth. This process, known as nutritional immunity, limits bacterial access to trace metals, including Fe ions (8). Inside the host, Fe is abundant, but it is typically found associated with proteins in prosthetic groups, including heme or Fe-S clusters. Non-cofactor-associated Fe, in large part, is ligated by proteins, including transferrin, lactoferrin, and calprotectin (4,9,10). Therefore, the “free” or loosely ligated Fe concentrations within host tissues are low to restrict pathogen growth (11). Hosts further limit Fe availability during infection by reducing the absorption of dietary Fe in a process referred to as anemia of inflammation (12). Pathogen-containing macrophages export Fe ions and increase the expression of ferritin to decrease free Fe titers (13,14). Individuals with the inborn disease hemochromatosis have increased Fe titers and an increased prevalence of infection, highlighting the importance of Fe limitation to prevent infection (15).

Given the scarcity of Fe in host tissues, bacteria must alter their gene expression profiles to colonize tissue and promote infection. A key part of the response to low Fe is the upregulation of Fe uptake systems, including the expression of siderophores, which are high-affinity extracellular Fe ion chelating molecules that can compete with host proteins for Fe ions (16). Once bound to Fe, siderophores are transported back into the cell via specific surface receptors. Other strategies for Fe uptake include the use of cell-wall associated transferrin binding proteins, monovalent Fe uptake, and acquisition of Fe from host hemoglobin (17).

In *S. aureus*, the ferric uptake transcriptional regulator (Fur) and partner Fpa sense and respond to cytosolic Fe titers (11,18). When associated with Fe, Fur typically acts as a transcriptional repressor (19,20). Growth in a low Fe medium promotes Fur demetallation, altered affinity for DNA, and expression of the Fur regulon. RegPrecise 3.0 predicts that there are 20 ORFs or operons in *S. aureus* that contain consensus Fur binding sites in their operators (21). In large part, these are genes involved in Fe uptake or storage. A *S. aureus* Δ*fur* mutant, or growth during Fe limitation, increases and decreases glycolysis and tricarboxylic acid (TCA) cycle expression, respectively (19,22). The mechanism behind the Fur-dependent regulation of central metabolic pathways in *S. aureus* has remained elusive, but a recent study suggests that IsrR plays a role (23).

In *Escherichia coli* and *Bacillus subtilis*, Fur directly controls the transcription of *ryhB* and *fsrA*, respectively (24,25). Both loci produce small non-coding regulatory RNAs (sRNA) that modulate gene expression by directly pairing with several messenger RNA (mRNA). In doing so, these sRNAs alter metabolism to spare Fe ions and redirect usage to prioritize essential processes. A recent publication demonstrated that the sRNA IsrR (originally named Tsr25 (26)) was required for growth during divalent metal starvation, suggesting that it is a functional analog of RyhB or FsrA (27). The expression of IsrR resulted in decreased expression of Fe-dependent enzymes formate dehydrogenase (*fdhA*) and glutamate synthase (*gltB2*). A direct interaction was noted between IsrR and the *fdhA* transcript *in vitro*. The *isrR* locus was initially identified in a global transcriptomic analysis as the most upregulated sRNA in human serum (26). Consistent with a role in pathogenesis, an Δ*isrR* mutant caused decreased mortality in a murine septicemia model (27).

S. aureus relies on appropriate metabolic adaptation to host encountered stresses such as iron limitation (19). Additionally, central metabolism and TCA cycle function impact virulence factor production and infection (28,29). This study was initiated to determine why a *S. aureus* Δ*fur* mutant has decreased expression of the TCA cycle enzyme aconitase. We demonstrate that IsrR modulates the expression of *acnA* and directly interacts with the *acnA* mRNA transcript. IsrR also alters the expression of additional genes coding TCA cycle enzymes. We demonstrate that Fur and IsrR contribute to cellular iron homeostasis and virulence using murine infection models of skin and pneumonia.

Materials and methods

Chemicals, bacterial strains, and growth conditions

Unless specified, the *S. aureus* strains used in this study (Table 1) were isogenic and constructed in the community associated *S. aureus* MRSA strain USA300_LAC that was cured of the native plasmid pUSA03 that confers erythromycin resistance (30). All bacteria were grown at 37 °C in tryptic soy broth (TSB) (MP Biomedicals) or a chemically defined medium containing the 20 canonical amino acids with or without 10 mM glucose (3). Solid tryptic soy agar (TSA) and chemically defined media were generated by adding 1.5 % (w/v) agar (VWR). Liquid cultures were shaken at 200 rpm. TSB treated with Chelex 100 resin (Bio-Rad) was prepared as previously described (31). Unless stated otherwise, cells were cultured in 10 mL capacity culture tubes containing 2.0 mL of liquid medium. Liquid phenotypic analysis was conducted in 96-well microtiter plates containing 200 µL of media per well using a BioTek 808E visible absorption spectrophotometer with continuous shaking at shake speed high. The optical density of cultures was measured at 600 nm (A_{600}). For quantitative growth, strains were grown overnight and washed with PBS before diluting to an optical density (A_{600}) of 0.05 in 200 µL of media. For spot plate growth analyses using solid media, strains were cultured for 18 hours in TSB before harvesting by centrifugation. Cells were washed with PBS, standardized to an optical density of 2 (A_{600}), serially diluted in PBS, and 5 µL aliquots were spotted upon solid media. Iron salts were added as ferrous sulfate.

Antibiotics were added at the following final concentrations: 100 µg mL^{-1} ampicillin (Amp); 10 µg mL^{-1} chloramphenicol (Cm) to select for plasmids and 3.3 µg mL^{-1} Cm to maintain plasmids (called TSB-Cm); 5 µg mL^{-1} erythromycin (Erm); 3 µg mL^{-1} tetracycline (Tet); 100 ng mL^{-1} anhydrotetracycline (Atet). Protein concentrations were determined using Bradford reagent (Bio-Rad Laboratories Inc., Hercules, CA). Unless stated otherwise, all chemicals were purchased from Sigma-Aldrich (St. Louis, MO).

Plasmid and strain construction

The restriction minus strain *S. aureus* RN4220 was used for transformations (32) and transductions were done using bacteriophage 80α (33). 5α Competent *Escherichia coli* (NEB) cultured in lysogeny broth was used for plasmid preparation.

Synthetic DNA (Table S2) was synthesized by Twist Biosciences (San Francisco, CA) and DNA primers (Table S1) were synthesized by Integrated DNA Technologies (Coralville, IA). Plasmids are listed in Table 2. Quick Ligase, restriction enzymes, competent *E. coli*, and HiFi DNA Assembly kit were purchased from New England Biolabs (NEB). All bacterial strains were PCR or sequence verified before use. Plasmid DNA and PCR products were sequenced by Azenta Life Sciences (South Plainfield, NJ).

The pJB38_Δ*isrR* was constructed by combining two digested PCR amplicons corresponding to the DNA upstream and downstream of the *isrR* locus with digested pJB38. The upstream region of *isrR* was amplified using primer pair tsr25 AF and tsr25 AR. The downstream region was amplified using primer pair tsr25 BF and tsr25 BR. pJB38 was digested using SacI and KpnI. The upstream amplicon was digested with SacI and MulI. The downstream region was digested with MulI and KpnI.

The pEPSA5_*isrR* complementation vector was created using the tsr25 pEPSA 5 EcoRI and tsr25 pEPSA 3 SalI primer pair with JMB1100 as template DNA. The

pEPSA5_as_*isrR* complementation vector was created using the tsr25 pMAL 5 SalI and tsr25 pMAL 3 EcoRI primer pair with JMB1100 as template DNA. The pEPSA5_*isrR** vector was created using the tsr25* pEPSA 5 EcoRI and tsr25 pEPSA 3 SalI primer pair with JMB10495 cells as template DNA. The pEPSA5_trunk_*isrR* was created using the tsr25 trunk pEPSA 5 EcoRI and tsr25 pEPSA 3 SalI primer pair with JMB1100 cells as the DNA template. The pEPSA5_*acnA* expression vector was created using the pEPSA5_acnAEcoRI (acnA RBS) and pEPSA_acnA3SalI primer pair. All pEPSA5 vectors were digested with EcoRI and SalI.

The pLL39_*isrR* complementing plasmid, pLL39_*isrR_C1*, pLL39_*isrR*_C2, and pLL39_*isrR_C1_C2* were created using the Tsr25 comp 5 SalI and Tsr25 comp 3 BamHI primer pair with JMB1100, synthetic DNA *isrR_C1,* synthetic DNA *isrR*_C2, and synthetic DNA *isrR_C1_C2* used as template DNA, respectively. All pLL39 vectors were digested with SalI and BamHI. The pLL39_*isrR*_C2a plasmid was generated by site-directed mutagenesis using the pLL39_*isrR* as DNA template, the SDM_IsrR_a_FWD and SDM_IsrR_a_REV primer pair and the Q5 Site-Directed Mutagenesis Kit (NEB).

The pOS_p*isrR_gfp* and pOS_p*isrR**_*gfp* transcriptional reporters were constructed using the pOStsr25_2forHindIII and pOStsr25_2revkpnI primer pair with JMB1100 and JMB10495 cells as template DNA, respectively. PCR products were digested and ligated into KpnI and HindIII digested pOS_*saeP1_gfp*.

The pOS_p*lgt_acnA_gfp*, pOS_p*lgt_acnA*1_*gfp* and pOS_p*lgt_acnA*2_*gfp* translational reporters were generated using pOS_p*lgt* digested with NdeI. The aconitase insert of pOS_p*lgt_acnA_gfp* was created using the plgt_acnA and acnA_gfp Wt A rev primer pairs with JMB1100 as template DNA. The *gfp* insert of pOS_p*lgt_acnA_gfp* was created using the acnA_gfp wt A for and gfp_plgt rev primer pair with the pOS_*saeP1_gfp* plasmid as template DNA. The aconitase insert of pOS_p*lgt_acnA1_gfp* was created using the plgt_acnA and acnA_gfp MutC rev primer pair with JMB1100 as template DNA. The *gfp* insert of pOS_p*lgt_acnA1_gfp* was created using the acnA_gfp MutC for and gfp_plgt rev primer pair with the pOS_*saeP1_gfp* plasmid as template DNA. The aconitase insert of pOS_p*lgt_acnA*2_*gfp* was created using the plgt_acnA and acnA_a Rev primer pair with JMB1100 as template DNA. The *gfp* insert of pOS_p*lgt_acnA2_gfp* was created using the acnA_a For and gfp_plgt rev primer pair with the pOS_*saeP1_gfp* plasmid as template DNA. All digested pOS_p*lgt* vectors, *acnA*, and *gfp* inserts were ligated using the NEB Hifi DNA Assembly Master Mix.

RNA extraction, cDNA synthesis and qPCR

To analyze RNA abundances corresponding to *isrR*, *S. aureus* strains were cultured overnight and diluted into 2 mL TSB to an optical density (A_{600}) of 0.1 in 10 mL culture tubes. The cell cultures were incubated with shaking until an A_{600} of 0.5 before 1 mL of cells was harvested by centrifugation, washed with PBS, and resuspended in 500 µL RNAprotect (QIAGEN).

To analyze *isrR* transcript stability, the Δ*fur::tetM* Δ*isrR* strain containing pEPSA5_*isrR* or pEPSA5_*isrR** were cultured overnight in TSB with 10 µg mL^{-1} chloramphenicol in 10 mL culture tubes at 37 °C with shaking. Cultures were diluted into 5 mL of fresh TSB with 10 µg mL^{-1} chloramphenicol and 2% xylose to an A_{600} of 0.1 in 30 mL culture tubes. The cells were cultured with shaking until an A_{600} of 0.5. Next, 1.5 mL of culture were added to 10 mL culture tubes containing rifampicin (100 µg mL^{-1}) and incubated with shaking at

37 °C. Cells were harvested at indicated time points by centrifugation, washed with PBS, and resuspended in 500 µL RNAprotect (QIAGEN). RNA extraction, cDNA synthesis, and transcript quantification (QuantStudio 3, Bio-Rad Laboratories Inc., Hercules, CA) were performed as previously described (31).

Northern blot analyses

RNA (3 µg/lane) was loaded onto a formaldehyde agarose gel and electrophoresed for 1 h 30 min at 120 V. RNAs were transferred onto a positively charged nylon membrane overnight by capillary transfer with 20 x SSC (1x SCC is 0.15 M NaCl plus 0.015 M sodium citrate) buffer and UV-crosslinked to the membrane. The presence of rRNA and ladder bands were visualized by staining the membrane with methylene blue (0.04 % in 0.5 M acetate solution). To detect *isrR*, a radio-labeled probe was made as follows: PCR targeting *isrR* using primers isrR5north and isrR3north was performed and the PCR mixture was radiolabeled using the Roche random prime labeling kit. Approximately 1 µg of PCR product was used with [α-32P] ATP according to the manufacturer's protocol. Probes were purified using Illustra MicroSpin G-25 columns (GE Healthcare). Membranes were prehybridized overnight at 45 °C in ULTRAhyb-Oligo buffer (Thermo Scientific) and then incubated with radiolabeled probe overnight at 45°C. After incubation, membranes were washed with 2×, 1×, and 0.5× SSC buffer and visualized using a phosphor imager screen.

Suppressor screen, genome sequencing, and SNP mapping

Ten independent cultures of the Δ*fur::tetM* strain (JMB10842) were grown overnight in 2 mL of TSB in 10 mL capacity culture tubes. One mL of cells was pelleted by centrifugation, resuspended in 1 mL PBS, and then diluted 1:100 in PBS. One hundred µL of the dilution was spread on chemically defined agar media containing amino acids without glucose. One colony from each plate (i.e. one per culture for ten total) was retained and struck for isolation. The increased growth phenotypes were verified by serially diluting cultures and spot plating them on solid defined amino acid media with and without glucose. We repeated the assay for a second time with five independent overnight cultures for a total of 15 suppressed strains.

For chromosomal DNA isolation, the Δ*fur::tetM* suppressed strains and the Δ*fur::tetM* parent strain were cultured overnight in 2 mL of TSB and genomic DNA was purified using the MaterPure Gram positive genomic DNA purification kit (LGC Biosearch Technologies). DNA was sequenced by SeqCenter (Pittsburgh, PA, USA) using Illumina technology.

Whole genome sequencing data was analyzed using the CLC Genomics Workbench software package (Qiagen). Reads were aligned to the *S. aureus* genome, using the USA300_FPR3757 genome sequence as a reference, as previously described (34). Quality-based variant detection was then performed to identify polymorphisms in each strain. A minimum threshold detection frequency of 80% was employed. The lists of polymorphisms generated for each suppressor mutant strain were cross-referenced against the parental strain (JMB10842). Common polymorphisms were eliminated (as were polymorphisms in homopolymeric nucleotide tracts) resulting in the identification of specific genetic variations between the suppressor strains and parental strain. The SNP in the promoter of the *isrR* gene was confirmed in the suppressed strains using Sanger

sequencing. These strains were referred to as Δ*fur isrR** and JMB10495 was used as a representative strain.

Transcriptional reporter assays

Overnight cultures of *S. aureus* strains containing a plasmid-based transcriptional reporter were cultured overnight in 2 mL TSB supplemented with 3.3 µg mL^{-1} chloramphenicol in 10 mL culture tubes at 37 °C with shaking. Cultures were then diluted to an optical density (A_{600}) of 0.05 in triplicate into 2 mL TSB supplemented with 3.3 µg mL^{-1} chloramphenicol +/- 250µM DIP in 10 mL culture tubes and incubated at 37 °C with shaking for 16 hours. Optical density (A_{600}) and GFP fluorescence (excitation 485 nm, emission 520 nm) were measured in microtiter plates using a Varioskan Lux plate reader (Thermo Scientific).

EMSA assays

PCR fragments containing T7-*acnA* (from -41 to +541), T7-*citM* (from -46 to +725), T7-*citZ* (from -41 to +850), T7-*lukH* (from -100 to +807), T7-*mqo* (from -248 to +328), and T7-*sdhC* (full-length, from -260 to +615) were used as DNA template for in vitro transcription with T7 RNA polymerase. RNAs were finally purified and radiolabeled when required as previously described (35).

5'-radiolabelled IsrR (20,000 cpm/sample, concentration <1 pM) and above-mentioned cold RNAs were separately denatured at 90°C in the buffer GR- (20 mM Tris-HCl pH 7.5, 60 mM KCl, 40 mM NH_4Cl, 3 mM DTT), cooled 1 min on ice, and incubated at room temperature for 15 min in presence of 10 mM $MgCl_2$. Renatured RNAs were then mix and incubated at 37°C for 15 min. Finally, samples were loaded on a 6% polyacrylamide gel under non-denaturing conditions (300 V, 4°C). Results are representative of two independent experiments.

Enzyme assays

Aconitase assays. Aconitase (AcnA) assays were conducted as previously described (36). Briefly, strains were cultured overnight in 2 mL of TSB with or without 10 µg mL^{-1} Cm before diluting them to an optical density (A_{600}) of 0.05 in 2 mL of TSB in 10 mL culture tubes . For strains containing pEPSA5, strains were cultured in TSB supplemented with 0.25 % or 2 % xylose for pEPSA_*acnA* and pEPSA_*isrR* containing strains respectively, and 3.3 µg mL^{-1} Cm. Strains were cultured with shaking at 200 rpm at a 45 degree angle for 16 hours. After incubation, one mL of cells was pelleted down and washed twice with PBS. After assaying AcnA activity as previously described (37), protein concentrations were determined using Bradford protein colorimetric assay modified for 96-well plate (Bio-Rad Protein Assay Dye Reagent Concentrate).

Succinate dehydrogenase assays. Succinate dehydrogenase (Sdh) assays were conducted as previously described (38). Cells were cultured and lysed as described for AcnA assays. The oxidation of succinate by succinate dehydrogenase was followed spectrophotometrically using the redox dye 2,6-dichlorophenol indophenol. The reaction mixture (1 mL) contained: potassium phosphate buffer (0.1 M, pH 7.4), KCN (3 mM), 2,6-dichlorophenol indophenol (DCPIP, 25 µM), *N*-methylphenazonium methosulphate (2.2 mM), succinic acid (20 mM, pH 7) and 20 µL of cell lysate. The reduction of DCPIP (molar extinction coefficient 21 mM^{-1} cm^{-1}) was followed at 600 nm for two minutes after addition

of all reagents as described (39). The succinate dependent slope (difference between the slope of absorbance/time of the sample with succinate minus the slope of the sample without succinate) was used to calculate specific Sdh activity. Protein concentrations were determined as described for the aconitase assay.

$$Specific\ succinate\ dehydrogenase\ activity\ (\frac{\mu mol}{min}) = \frac{\frac{succinate\ dependent\ slope}{21 mM^{-1}\ cm^{-1}}}{total\ protein\ in\ cell\ free\ extract}$$

Malate quinone oxidoreductase assays. Cells were cultured and lysed as described for AcnA assays. Reaction mixture was the same as described for Sdh assays except for the use of sodium malate (20 mM) instead of succinic acid.

Streptonigrin sensitivity

Cells were cultured overnight and diluted to an optical density (A_{600}) of 0.05, after which 100 µL of the dilute culture was added to 4 mL of soft TSB agar (0.3 % wt vol^{-1}) and overlaid on TSA media. After soft agar solidified, 2.5 µL of streptonigrin (1 mg mL^{-1}) was spotted. Zone of clearance was measured after one day incubation at 37°C.

CAS siderophore assay

Overnight cultures in TSB were diluted 100-fold into 1 mL of Chelex (Bio-Rad)-treated TSB with the addition of 25 µM zinc acetate, 25 µM $MnCl_2$, 1 mM $MgCl_2$ and 100 µM $CaCl_2$ in 10 mL glass culture tubes. The cultures were incubated at 37 °C with shaking for 18 hours. The chrome azurol S siderophore assay was performed on the spent media using the modified microplate method as previously reported (40,41).

Whole cell metal quantification

S. aureus strains were grown for 18 hours overnight in TSB before diluting them to an optical density (A_{600}) of 0.05 into 7.5 mL of TSB or Chelex-treated (Bio-Rad) TSB in 30 mL capacity culture tubes as described previously (31). Cells were allowed to grow with shaking for eight hours. Pre-weighted metal-free 15 mL propylene tubes were used to pellet the cells in a tabletop centrifuge at 4 °C (Eppendorf, Hauppauge, NY). Pellets were washed three times with 10 mL of ice-cold PBS. Samples were kept at -80 °C or on dry ice until processing.

Cell pellets were acid digested with 2 mL of Optima grade nitric acid (ThermoFisher, Waltham, MA) and 500 µL hydrogen peroxide (Sigma, St. Louis, MO) for 24 hr at 60 °C. After digestion, 10 mL of UltraPure water (Invitrogen, Carlsbad, CA) was added to each sample. Elemental quantification on acid-digested liquid samples was performed using an Agilent 7700 inductively coupled plasma mass spectrometer (Agilent, Santa Clara, CA). The following settings were fixed for the analysis Cell Entrance = −40 V, Cell Exit = −60 V, Plate Bias = −60 V, OctP Bias = −18 V, and collision cell Helium Flow = 4.5 mL min^{-1}. Optimal voltages for Extract 2, Omega Bias, Omega Lens, OctP RF, and Deflect were determined empirically before each sample set was analyzed. Element calibration curves were generated using ARISTAR ICP Standard Mix (VWR). Samples were introduced by a peristaltic pump with 0.5 mm internal diameter tubing through a MicroMist borosilicate glass nebulizer (Agilent). Samples were initially up taken at 0.5 rps for 30 s followed by 30 s at 0.1 rps to stabilize the signal. Samples were analyzed in

Spectrum mode at 0.1 rps collecting three points across each peak and performing three replicates of 100 sweeps for each element analyzed. Sampling probe and tubing were rinsed for 20 s at 0.5 rps with 2% nitric acid between each sample. Data were acquired and analyzed using the Agilent Mass Hunter Workstation Software version A.01.02.

Murine models of infection

Acute pneumonia model. Experiments were conducted as previously described (42). Briefly, mice were intranasally infected with 2-4 x 10^7 colony forming units (CFU) in 50 µL of PBS under anesthesia (ketamine and xylazine). Bacterial loads were enumerated at 24 h post infection from bronchoalveolar lavage fluid (BALF) by washing the airway 3 times with 1 mL of PBS, and homogenized lung tissue. Bacterial counts were quantified by serial dilution using CHROMagar *S. aureus* plates (BD Biosciences).

Skin and soft tissue model. All studies were conducted in accordance with an approved protocol at The University of Kansas Medical Center. Female C57BL/6J mice (Jackson Laboratories) were used in a subcutaneous skin infection model as previously described (43). Briefly, 8-week-old mice were injected with ~2.1e7 CFU of mid-exponential phase cells suspended in PBS. Mice were imaged daily, and lesion sizes determined using ImageJ. On the final day, mice were euthanized and the lesion plus ~3 mm of neighboring tissue were homogenized in 1X HBSS 0.2% HAS 10 mM HEPES buffer using an MP Biomedicals Fastprep-24 homogenizer with Lysing Matrix H tubes following the manufacture's protocol for skin. A sample was taken to determine bacterial titers by dilution plating. Next, the samples were clarified by centrifugation, treated with 1x protease inhibitor (Roche), and frozen at -80 °C until processed for cytokines. Cytokines were measured using the BD cytometric bead array (CBA) mouse flex set protocol on a BD Aria flow cytometry machine and analyzed in FCS express.

Ethics statement

Animal work in this study was carried out in strict accordance with the recommendations in the Guide for the Care and Use of Laboratory Animals of the NIH (National Academies Press, 2011), the Animal Welfare Act, and US federal law. Protocols were approved by the Institutional Animal Care and Use Committee of Rutgers New Jersey Medical School of Newark, New Jersey, USA, as well as The University of Kansas Medical Center, Kansas City, Kansas, USA.

Statistical analysis

For two group comparisons (controls vs treatment or between bacterial strains), student's t-tests were performed. Multiple group comparisons for animal data were performed using an ANOVA with a Kruskal-Wallis test or a Mann-Whitney non-parametric test for two group comparisons. All analyses were conducted with Sigmaplot 11, Microsoft Excel, or Prism 9.

Results

Iron starvation decreases aconitase activity in a Fur-dependent manner.

Previous work demonstrated that both the absence of Fur in *S. aureus* or Fe depletion resulted in a redirection of central metabolism where glycolysis is increased, and the TCA cycle is downregulated (24,25). The shift towards fermentative metabolism increases Fe availability, and since the TCA cycle contains Fe-S cluster requiring enzymes, its downregulation could be a way to decrease nonessential Fe usage in an Fe-sparing response (19,44).

We tested the hypothesis that the Fe-S cluster requiring enzyme aconitase (AcnA), which converts citrate to isocitrate in the TCA cycle, would have decreased activity upon Fe limitation. We quantified the activity of AcnA in the parent strain, USA300_LAC, and the isogenic Δ*fur::tetM* (Δ*fur*) mutant. The strain lacking Fur had nearly undetectable AcnA activity, and the phenotype could be genetically complemented (Fig 1A). The divalent metal chelator 2,2'-dipyridyl (DIP) has a high affinity for Fe(II) and co-culture with DIP results in Fur derepression (44,45). When the WT strain was co-cultured with DIP, the activity of AcnA was significantly decreased (Fig 1B).

We examined whether decoupling *acnA* transcriptional activity from its native promoter would increase AcnA activity in the *fur* mutant. To this end, we placed *acnA* and its ribosomal binding site (RBS) under the transcriptional control of a xylose inducible promoter (*xylRO*) using the pEPSA5 plasmid. We examined AcnA activity in the extracts of the *acnA::Tn* and *acnA::Tn* Δ*fur* strains containing pEPSA5_*acnA* after culture with xylose. The *acnA::Tn* Δ*fur* strain had significantly decreased AcnA activity compared to the *acnA::Tn* strain (Fig 1C). These data demonstrate that *acnA* expression is altered in a strain lacking *fur* and this regulation is also independent of its native promoter.

S. aureus requires a functional TCA cycle to use amino acids as carbon and energy sources (36,46). We compared the growth of the WT, Δ*fur*, and *acnA::Tn* strains cultured in a chemically defined medium containing amino acids with and without glucose. The Δ*fur* and *acnA::Tn* strains had severe growth defects in the medium containing amino acids as the sole carbon and energy source, whereas the WT was capable of growth (Fig 1D). All three strains were capable of growth when the medium was supplemented with glucose (Fig 1E). We also found that the Δ*fur* and *acnA::Tn* strains did not grow on a solid chemically defined medium containing amino acids for carbon and energy. Again, this phenotype was reversed by supplementing the medium with glucose (Fig S1).

A null mutation in *isrR* promotes the growth of a Δ*fur* strain on amino acids.

We conducted suppressor analysis to provide insight into the defective growth of the Δ*fur* strain on an amino acid medium. We individually plated fifteen cultures of the Δ*fur* strain on a chemically defined solid medium containing only amino acids as carbon and energy sources. We isolated one colony from each plate, verified the phenotype of improved growth with amino acids, and then determined the locations of the single nucleotide polymorphisms by whole genome sequencing. All fifteen strains contained a C→T mutation located 604 base pairs upstream of the translation start site of *arlR* (SAUSA300_1308). This chromosomal location corresponds to *tsr25* (recently renamed *isrR*), which codes for a sRNA (26,27). The mutations correspond to a G→A change within the *isrR* sequence at the +1 from the transcriptional start site as determined by RNA

sequencing (47) and the +3 location as determined by 5' RACE analysis (27). Henceforth, we refer to this allele as *isrR**. The *isrR** mutation permitted the growth of the Δ*fur* mutant on both solid and liquid chemically defined amino acid media (Fig 2A and Fig S2). The Δ*fur isrR** strain also had increased AcnA activity compared to the Δ*fur* mutant (Fig 2B).

Three findings suggested that the *isrR** allele decreased IsrR function and thereby corrected the phenotypes of the Δ*fur* strain. First, we linked a transposon (Tn) (SAUSA300_1309::Tn) to the *isrR** mutation and then used this strain as a DNA donor for transduction into the Δ*fur* strain. We isolated two classes of transductants. One class corrected the growth of the Δ*fur* mutant on amino acid media, and the second class did not. Sanger sequencing determined that the strains that grew on amino acid medium contained the *isrR** allele, and all strains that did not grow contained the wild type *isrR* allele. Second, we constructed Δ*isrR* and Δ*fur* Δ*isrR* strains. Deletion of *isrR* in the Δ*fur* strain permitted growth on solid and liquid defined amino acid medium (Fig 2C and Fig S3). Deletion of *isrR* in the Δ*fur* strain also increased AcnA activity (Fig 2D). Introduction of the *acnA::Tn* mutation into the Δ*fur* Δ*isrR* strain prevented growth in amino acid medium consistent with the hypothesis that the increased growth imparted by the null *isrR* mutations requires functional AcnA (Fig 2C and Fig S3). Third, we genetically complemented the Δ*isrR* strains. The pLL39 episome codes for tetracycline resistance so we could not use the Δ*fur* strain. Instead, we used previously described strains containing a null $fur_{E11stop}$ allele (*fur**) that is genetically linked to a transposon in gene SAUSA300_1456 (18). As expected, the strain containing *fur** had greatly reduced AcnA activity. The presence of the Δ*isrR* mutation in the *fur** strain increased AcnA activity and growth on chemically defined amino acid medium, and the phenotypes could be genetically complemented (Figs 2D and S4).

We also examined the effect of the Δ*isrR* mutation on AcnA activity when *acnA* was expressed from a non-native promoter. We quantified AcnA activity in cell lysates generated from the *acnA::Tn*, *acnA::Tn* Δ*fur*, and *acnA::Tn* Δ*isrR* Δ*fur* strains containing pEPSA5_*acnA* after culture in tryptic soy broth (TSB) containing xylose (Fig 2E). Again, the activity of AcnA was decreased in the strain lacking Fur, and the introduction of the Δ*isrR* mutation increased AcnA activity, but not to the level of that in the parent strain.

The *isrR allele decreases *isrR* transcription.**

The *isrR* promoter contains two near consensus Fur box sequences (27). The *isrR** mutation resulted in a base change in the Fur box proximal to the *isrR* transcription start site (Fig 3A). We conducted Northern blot analyses to 1) determine if *isrR* transcript abundances responded to divalent metal starvation, and 2) verify that it was regulated by Fur in USA300_LAC. The *isrR* transcript increased in abundance in the WT as we increased the concentration of DIP in the growth medium but was not detected in the Δ*isrR* strain (Fig 3B and S5). Moreover, the *isrR* transcript accumulated in the Δ*fur* strain when compared to the unchallenged WT strain, but there was no additional accumulation in the Δ*fur* strain upon co-culture with DIP (Fig 3B). The isrR transcript was not detectable in the Δ*isrR* Δ*fur* strain. These data are consistent with previous results demonstrating that *isrR* transcription is regulated by Fur (27) and suggest that Fur is the dominant divalent metal-dependent transcriptional regulator controlling *isrR* transcription.

To evaluate how the *isrR** mutation was affecting the expression of *isrR*, we used Northern blot analysis and quantitative PCR to examine the abundances of the transcripts

corresponding to *isrR* in the WT, Δ*fur*, and Δ*fur isrR** strains after culture in the presence and absence of DIP. We could detect the *isrR* transcript in the Δ*fur isrR** strain, and the basal expression in unchallenged cells appeared to be increased compared to the WT (Fig 3B). However, *isrR* did not appear to be significantly induced in the Δ*fur isrR** strain by co-culture with DIP.

We quantified these findings using qPCR. The abundance of the *isrR* transcript was increased in the WT upon co-culture with DIP (Fig 3C). The *isrR* transcript was elevated in the Δ*fur* strain when compared to the WT, and it did not further increase in abundance upon co-culture with DIP. The abundance of *isrR* transcripts in the Δ*fur isrR** strain was slightly higher than the WT when unchallenged; however, the *isrR* transcript abundance did not significantly increase in the Δ*fur isrR** strain upon co-culture with DIP. These data suggest that the *isrR** mutation decreases the transcriptional activity of the *isrR* locus under iron starvation or that it promotes decreased IsrR transcript stability.

We tested the hypothesis that the *isrR** mutation was suppressing the defects of the Δ*fur* strain by decreasing IsrR stability. We cultured the Δ*fur* Δ*isrR* strain containing pEPSA5_*isrR* or pEPSA5_*isrR** in the presence of xylose to induce *isrR* transcription. We then added rifampicin to inhibit RNA synthesis, isolated samples at different time points, and quantified *isrR* transcripts. The transcripts corresponding to *isrR* and *isrR** decayed at similar rates. In fact, the *isrR** transcript had a higher relative abundance than the *isrR* transcript 30 minutes after transcription was halted (Fig 3D).

We next tested the hypothesis that the *isrR** mutation was suppressing the defects of the Δ*fur* strain due to decreased *isrR* transcription. We generated transcriptional reporter constructs where the *isrR* or *isrR** promoter drove transcription of *gfp*. The WT strain containing either construct was cultured in TSB with and without DIP, and *gfp* fluorescence was quantified. Co-culture with DIP significantly increased *gfp* expression in both strains containing a transcriptional reporter (Fig 3E). However, the strain containing the *isrR*_gfp* had considerably decreased *isrR* transcriptional activity upon Fe-depletion compared to the strain expressing *isrR_gfp.*

We individually placed the expression of *isrR*, *isrR**, antisense *isrR* (as_*isrR*), and a truncated *isrR* that begins two nucleotides downstream from the nucleotide mutated in *isrR** (trunk_*isrR*), under the transcriptional control of *xylRO* promoter using pEPSA5. Induced expression of *isrR*, *isrR**, or trunk_*isrR* in the WT strain significantly decreased AcnA activity and decreased growth on solid defined media compared to the WT strain containing the empty vector (Figs 3F and S6). The AcnA activity or the growth of WT expressing the as_*isrR* was not significantly different to that of the WT containing the empty vector. These results suggest that 1) the expression of *isrR* under metal-replete conditions decreases *acnA* expression, and 2) the *isrR** mutation does not affect the ability of the *isrR** transcript to decrease *acnA* expression. These findings are consistent with the hypothesis that the *isrR** mutation results in decreased transcription of the *isrR* locus and, thereby, suppresses the phenotypes of the Δ*fur* strain.

The presence of IsrR results in decreased *acnA* expression.

Our results are consistent with a model wherein the absence of Fur or upon Fe ion limitation, *isrR* is expressed and mediates the repression of *acnA* expression. We tested the hypothesis that IsrR alters *acnA* expression post-transcriptionally. We used data from a published RNA-sequencing dataset to observe the length of the *acnA* 5' untranslated

region (UTR) and estimate that it extends -41 bases from the translational start site under the growth conditions examined (Fig S7)(26). We used the program IntaRNA (Freiburg RNA tools (48,49)) to help predict potential interactions between IsrR and the *acnA* transcript. One potential interaction site was identified that overlayed the 5' UTR and the first two codons of the coding sequence with a base-pair minimal annealing energy of -14.2 kcal mol^{-1}. This interaction included a 100% overlap with the Shine Dalgarno sequence (AGGGGG) (Fig 4A).

To evaluate the effect of IsrR on *acnA* translation, we created a translational reporter where the constitutive *lgt* promoter drove transcription of a chimeric *acnA_gfp* generated by fusing the *acnA* 5'UTR and first two *acnA* codons in frame with the coding sequence of *gfp* (pOS_p*lgt_acnA_gfp*). We used this construct to quantify *gfp* expression in the WT and Δ*isrR* strains after culture with and without DIP. The expression of *gfp* was decreased in the WT strain upon co-culture with DIP, but not in the Δ*isrR* strain (Fig 4B).

We next used the translational reporter to compare *gfp* expression in the WT, Δ*fur*, Δ*fur* Δ*isrR*, and Δ*fur isrR** strains. When compared to the WT strain, the expression of *gfp* was decreased in the Δ*fur* strain (Fig 4C). However, the presence of either the Δ*isrR* or *isrR** alleles reversed the Δ*fur* phenotype. These data are consistent with the hypothesis that IsrR modulates the expression of the *acnA_gfp* allele *in vivo*.

We tested the hypothesis that the *isrR* and *acnA* transcripts interact *in vitro*. We performed an electrophoretic mobility shift assay (EMSA) using labeled IsrR and the 5' of *acnA* transcript (from -41 to +541). RNA-RNA gel shifts demonstrated that titrating *acnA* transcript into samples containing IsrR decreased the rate at which IsrR migrated through the polyacrylamide matrix, suggesting a direct interaction between IsrR and the *acnA* transcript (Fig 4D). Using these data, we estimated that the K_d of IsrR for the *acnA* transcript is likely less than 50 nM. IntaRNA does not predict a strong interaction between IsrR and the *lukH* transcript, which codes for a leukotoxin. IsrR failed to interact with the *lukH* transcript using the same amounts of IsrR and *lukH* transcript as used for the *acnA* transcript EMSA (Fig 4E).

IsrR may interact with the *acnA* transcript ribosomal binding site.

To further analyze the predicted IsrR-*acnA* mRNA interaction, we modified the *acnA* translational reporter to contain base change substitutions in and around the *acnA* Shine Dalgarno sequence, which are predicted to interact with IsrR, but still allow RBS function (pOS_p*lgt_acnA1_gfp*) (Fig 5A). We hypothesized that these nucleotides were involved in IsrR-*acnA* mRNA interaction, and base substitutions would affect IsrR binding, thus decoupling *acnA_gfp* expression from IsrR control. We quantified *gfp* expression from the *acnA_gfp* and the mutated *acnA1_gfp* translational reporters in the WT, Δ*fur,* Δ*isrR,* and Δ*fur* Δ*isrR* strains. The *acnA_gfp* behaved as previously demonstrated, and the Δ*fur* mutant had decreased *gfp* expression, which was restored upon deletion of *isrR* (Fig 5B). The fluorescence from *acnA1_gfp* showed no significant differences between the strains examined, suggesting that the nucleotide substitutions in the *acnA* RBS decreased IsrR-mediated expression control.

Coronel-Tellez *et al*. determined that IsrR has cytosine-rich regions (CRRs), which may be used to bind mRNA targets (27). IntaRNA predicted individual interactions between the IsrR CRR_1 (Fig S8) and CRR_2 (Fig 4A) with the *acnA* transcript. We set out to determine if CRR_1 or CRR_2 is primarily responsible for driving the interactions

between IsrR and the *acnA* 5' UTR. We designed three different IsrR variants: one with mutations near CRR_1 (*isrR_C1*), one with mutations near the CRR_2 (*isrR_C2*), and one that combined both the CRR_1 and CRR_2 mutations (*isrR_C1_C2*) (Fig 5C). The mutated *isrR* variants and the wild type *isrR* were individually cloned into the pLL39 episome and integrated onto the chromosome of the Δ*isrR fur** strain (null *fur* allele). We then used the *acnA_gfp* translational reporter to quantify the effect of the *isrR* alleles on *gfp* expression. The Δ*isrR fur** strains carrying *isrR* or *isrR_C1* decreased *gfp* expression, suggesting that both alleles function to modulate the expression of *acnA_gfp* (Fig 5D). The expression of *acnA_gfp* in the strains carrying the *isrR_C2* or *isrR_C1_C2* alleles phenocopied the strain carrying the empty vector, suggesting that these *isrR* variants lost the ability to control *acnA_gfp* expression. We found that *isrR* transcript levels accumulated to similar levels in each strain, demonstrating that the difference in *acnA* translational activity did not result from differential IsrR accumulation (Fig S9).

We next monitored AcnA activity in cell lysates of the WT and Δ*isrR fur** strains carrying the empty vector or the different *isrR* alleles. The Δ*isrR fur** strains carrying *isrR* or *isrR_C1* decreased AcnA activity, suggesting that both alleles function to modulate *acnA* expression (Fig 5E). The activity of AcnA in the Δ*isrR fur** strains carrying the *isrR_C2* or *isrR_C1_C2* alleles behaved like the Δ*isrR fur** strain carrying the empty vector suggesting that these *isrR* variants lost the ability to control *acnA* expression. These findings are consistent with the hypothesis that the CRR_2 region of IsrR is utilized to interact with the *acnA* transcript and instigate translational repression.

We sought further confirmation that IsrR may interact with *acnA* transcript ribosomal binding site using CCR_2. We constructed an IsrR variant that contained a single base change in the CRR_2 (*isrR_C2a*) (Fig 6A). Expression of *isrR_C2a* in the Δ*isrR fur** strain resulted in increased aconitase activity compared to the strain expressing *isrR* (Fig 6B). The Δ*isrR fur** strain containing *isrR_C2a* also had increased *gfp* expression from the *acnA_gfp* transcriptional reporter compared to the strain expressing *isrR,* suggesting that the one base pair change in CRR_2 was sufficient to lessen IsrR regulatory control over *acnA_gfp* expression (Fig 6C). We next constructed an *acnA* translational reporter that contained a compensatory mutation intended to base pair with the mutation introduced in *isrR_C2a* (pOS_p*lgt_acnA2_gfp*) (Fig 6D). The Δ*isrR fur** strain containing *isrR* decreased expression of *acnA_gfp* compared to the parent strain, but not expression of *acnA2_gfp*, suggesting that the one base pair change decreased the ability of IsrR to regulate *acnA2_gfp* expression (Fig 6E). Importantly, the Δ*isrR fur** strain containing the *isrR_C2a* allele decreased *acnA2_gfp* expression, demonstrating that introducing a compensatory mutation into *isrR* regained some control over *acnA2_gfp* expression. The *isrR* and *isrRC2a* transcripts accumulated to similar levels in the Δ*isrR fur** strain (Fig S9).

IsrR represses the expression of additional genes coding TCA cycle enzymes.

We sought to determine whether IsrR also controls the expression of genes coding for additional TCA cycle enzymes. We used IntaRNA and identified predicted IsrR interaction sites in the 5'UTR of *sdhC* (succinate dehydrogenase), *citM* (citrate synthase), and *citZ* (citrate importer) (Figs S10, S11, S12). We also identified a site in *mqo* (malate quinone oxidoreductase) in the 5' region of the coding sequence (Fig S13). We performed RNA-RNA gel shifts to examine if IsrR could interact with the *sdh*, *mqo*, *citM*, or *citZ* transcripts

in vitro (Figs 6A-C). Gel shifts show IsrR directly interacts with all four transcripts with an estimated K_d that is less than 50 nM.

We next tested the hypothesis that IsrR would negatively regulate the expression of *sdh* and *mqo*. We cultured the WT, Δ*fur,* Δ*isrR,* and Δ*fur* Δ*isrR* strains in TSB and assessed the activities of succinate dehydrogenase (Sdh) and malate quinone oxidoreductase (Mqo) in cell-free lysates (Figs 6D-E). The Sdh and Mqo activities were decreased in the Δ*fur* mutant, and activity was partially restored upon the deletion of *isrR*. These results suggest that IsrR mediates the repression of both Fe-S cluster and non-Fe using TCA cycle enzymes in response to Fe limitation.

IsrR impacts iron ion homeostasis.

IsrR was demonstrated to downregulate the expression of non-essential Fe utilizing genes including *gltA, fdh, miaB,* and anaerobic nitrate respiration (*nasD* and *narG*) (27,50). This work also showed that IsrR is required for growth upon Fe depletion, leading to a model wherein IsrR contributes to Fe sparing upon Fur demetallation. TCA cycle enzymes are a cellular Fe sink, and herein, we demonstrate that IsrR represses the expression of TCA cycle genes in the absence of Fur*,* which contributes to the proposed Fe-sparing model.

We tested the hypothesis that *isrR* expression promotes Fe uptake and/or an increase in Fe ions not ligated by macromolecules (also called “free Fe”). The antibiotic streptonigrin, when combined with intracellular Fe(II) and a reducing agent, promotes killing by causing double-stranded DNA breaks (3,7). Therefore, increased killing by streptonigrin is correlated with an increased pool of Fe that is not chelated by macromolecules. We assayed streptonigrin sensitivity by spotting streptonigrin on top agar overlays containing the WT, Δ*fur,* Δ*isrR,* or Δ*fur* Δ*isrR* strains. The Δ*fur* strain displayed increased streptonigrin sensitivity compared to the WT (Fig 8A). This phenotype was expected since a Δ*fur* mutant has derepressed Fe uptake (18). The Δ*fur* Δ*isrR* had decreased streptonigrin sensitivity when compared to Δ*fur,* suggesting a role for IsrR in increasing streptonigrin sensitivity on a Δ*fur* strain. We confirmed a role for IsrR in increasing streptonigrin sensitivity by inducing the expression of *isrR* or an antisense *isrR* (as_*isrR*) in the WT strain using the pEPSA5 vector. Induced expression of *isrR*, but not as_*isrR*, resulted in increased streptonigrin sensitivity (Fig 8B). These data are consistent with the hypothesis that upon Fe limitation and Fur derepression, *isrR* expression increases the pool of free intracellular Fe.

We next evaluated the role of IsrR in Fe ion uptake. We quantified total ^{56}Fe pools using inductively coupled mass spectrometry (ICP-MS) after growth in 1) TSB, 2) TSB with 50 μM Fe(II), and 3) TSB treated with Chelex to decrease the titers of divalent metals (Figs 8C, 8D, 8E). The Δ*fur*, Δ*isrR*, and Δ*fur* Δ*isrR* strains had increased titers of ^{56}Fe compared to the WT in all three media. However, the Δ*isrR* and Δ*fur* Δ*isrR* strains had decreased ^{56}Fe levels compared to Δ*fur* in Chelex-treated TSB and TSB supplemented with Fe. The intermediate iron levels of the Δ*fur* Δ*isrR* suggest that IsrR contributes to the increased Fe levels in strains lacking Fur.

Lastly, we examined whether IsrR has a role in siderophore production and/or uptake. We quantified total siderophore production in the WT, Δ*fur,* Δ*isrR,* and Δ*fur* Δ*isrR* strains after culture in Chelex-treated TSB. The Δ*fur* strain had increased siderophore production compared to the WT (Fig 8F). The Δ*fur* Δ*isrR* double mutant strain produced fewer

siderophores than the Δ*fur*, but more than the Δ*isrR* and WT strains. Taken together, these findings verify a role for IsrR in the Fe ion homeostasis and suggest that it has a role in siderophore production.

IsrR and Fur contribute to *S. aureus* pathogenesis.

The connection between *S. aureus* metabolism and virulence potential is well described. Pathogenesis requires nutritional adaptation to the niche and altered virulence factor production is often linked to nutrient availability changes (51,52). *S. aureus* is one of the most common causes of bacterial pneumonia and the most common pathogen isolated in skin and soft tissue infections (53,54). Host-induced hypoferremia is a commonality in both bacterial lung and skin and soft tissue infections (55,56).

We first used a model of acute pneumonia to define the respective roles of IsrR and Fur in pathogenesis. In both bronchoalveolar lavage fluid (BALF) and lung tissue, we observed the importance of IsrR in pathogenesis (Fig 9A and 9B). While we did not observe a significant impact of Fur in this model, the inactivation of *isrR* led to a decrease in bacterial survival. In BALF, the inactivation of *isrR* led to a nearly 40-fold reduction in bacteria; this held true in the lung with a 25-fold decrease.

We next sought to determine how the absence of IsrR or Fur would impact skin infection. To this end, we performed a murine model of skin infection and monitored several outcomes. We observed no difference in lesion size between the Δ*isrR* mutant and WT strain (Fig 9C). By contrast, the lesion sizes significantly decreased for the Δ*fur* and Δ*fur* Δ*isrR* strains compared to the WT-infected mice. While lesion size reports the overall surface lesion, necrosis size quantifies fully necrotic tissue that forms during infection and is observed as a scab-like structure. The same trends were observed for necrosis between the strains (Fig 9D).

To determine if reduced lesion or necrosis size in the absence of Fur was due to changes in bacterial colonization, bacterial titers at the site of infection were determined at 4 days post-infection. We observed an approximately 3-fold decrease in bacterial titers in all mutant strain-infected mice compared to WT-infected mice at this time point (Fig 9E). Since the Δ*isrR* mutant showed reduced bacterial numbers but not decreased lesion formation, we interpret this to mean that the smaller lesions observed in the Δ*fur* and Δ*fur* Δ*isrR* strains are not likely due to changes in bacterial titers at the site of infection.

Tissue damage likely results from a combination of bacterial factors and the host's immune response. Considering the reduced tissue damage in the absence of Fur, we measured cytokine and chemokine levels at the site of infection to provide insight into the immunological changes occurring during infection with *fur* mutants. We used a panel of proinflammatory cytokines that are important for immune cell recruitment and/or activation. We did not observe a change in KC, MCP-1, GM-CSF, or MIP1α between the strains (Fig S14). Thus, tissue damage differences did not correlate with any changes in these chemokines and cytokines. IL-1β, G-CSF, and IL-6 were decreased in all mutant bacterial infections. In contrast, we observed increased IL-1α but decreased TNFα and G-CSF in a Fur-dependent manner, and these changes correlate with decreased lesion size when Fur was absent. We did not perform statistical analysis on CCL5 (RANTES), but while it was readily detectable in wild type-infected mice, most mutant mice had levels below the limit of quantification. The finding that some cytokine levels, but not others, differed when Fur was absent suggests specific immunological changes are occurring

during infection in a Δ*fur* mutant. What those changes are in immune cell recruitment or activation and the mechanism by which this occurs will require additional investigation.

Discussion

This study was initiated to understand why a strain lacking Fur has decreased TCA cycle function. Work by others led to the hypothesis that growth in Fe-limiting conditions decreases the levels of Fe-bound Fur, resulting in altered affinity for DNA and derepression of the Fur regulon (11,19). Bioinformatic work led us to predict that the genes that Fur directly regulates are utilized for Fe uptake and a gene for Fe storage (*dps*) (18). However, we discovered that a Δ*fur* mutant had greatly reduced AcnA activity. We also noted that neither Δ*fur* or *acnA::Tn* mutants could grow using amino acids as carbon or energy sources, providing us with a phenotype that we could exploit.

We used an unbiased suppressor screen approach to identify IsrR as the Fur-regulated negative regulator of aconitase expression. To our knowledge, this is the first case of a suppressor screen identifying an sRNA through the suppressive effects of a null mutation permitting growth on an otherwise non-permissive growth condition. This finding showcases the power of suppressor screen genetics and highlights the broad impacts that IsrR has on *S. aureus* physiology.

The suppressor mutations in *isrR* (called *isrR**) allowed for increased growth of the Δ*fur* mutant on defined amino acid media. Interestingly, all fifteen of the *isrR** mutant strains, isolated during two separate screening events, contained the same mutation in the operator of *isrR,* suggesting that there is something unique about this allele. In alternate organisms, small proteins, such as Hfq in *E. coli*, promote interaction between a sRNA and a target mRNA (57). The finding that suppressor mutations only mapped to the promoter of *isrR* and not to alternate loci, including *hfq*, suggests that *S. aureus* does not require a single protein to facilitate interaction between IsrR and target RNAs. The recent study by Coronel-Tellez *et al*. found that a strain with a deletion mutation in the gene predicted to code the Hfq homolog did not alter IsrR-dependent regulation of expression (27). Alternatively, there could be more than one chaperone that aids IsrR regulation that share functional overlap.

The *isrR* operator has two Fur-boxes and the *isrR** mutation is in the Fur-box that is proximate to the transcription start site (27). The mutation resulted in significantly reduced *isrR* transcription upon Fe depletion or in a Δ*fur* mutant. It also resulted in an inability for *isrR* transcription to be induced in a fur mutant during low Fe. The *isrR** mutation did not alter *isrR* transcript degradation, and strains expressing *isrR** or *isrR* using a non-native promoter resulted in phenotypic similarities, suggesting that *isrR** is functional *in vivo*, but the mutation decreases transcription.

The deletion of *isrR* increased the AcnA activity of a Δ*fur* mutant*,* and over-expression of *isrR* in the WT decreased AcnA activity. We identified a predicted IsrR binding site in the *acnA* transcript and demonstrated that IsrR interacted with the *acnA* transcript *in vitro*. The predicted interaction site overlayed the *acnA* Shine Dalgarno sequence. Introducing mutations into the Shine Dalgarno sequence of *acnA* that preserve the ribosomal binding site but impact predicted base-pairing with IsrR decreased IsrR-mediated control of *acnA* expression. Additionally, mutations impacting the second cytosine-rich region (CRR_2) of IsrR, predicted to interact with the *acnA* transcript, also decreased IsrR control over *acnA* expression. Lastly, we were able to change one base pair in the *acnA* RBS, resulting in decreased IsrR control over *acnA* expression. The introduction of a compensatory mutation into the CRR_2 sequence of IsrR resulted in a partially corrected ability of IsrR

to control *acnA* expression. While not definitive, these data are consistent with a model wherein IsrR binds the *acnA* transcript and mediates translational repression through occlusion of the RBS. This model is supported by previous findings where IsrR mediates translational repression of *fdhA* and *gltB2*, which have similar predicted IsrR pairing sites as the *acnA* transcript and don't appear to trigger mRNA degradation (27).

The introduction of the Δ*isrR* mutation to the Δ*fur* strain resulted in only partial recovery of AcnA activity. The *acnA* promoter contains a Fur box terminating at position -179. We are currently trying to determine if Fur directly acts as an activator of *acnA* transcription. While this manuscript was in revision, a manuscript was published that also demonstrated that IsrR controls *acnA* expression in *S. aureus* (58). The authors also demonstrated that AcnA, when not ligating an FeS cluster, can bind to mRNA transcripts, directly decreasing the expression of *acnA* (*citB*), *citZ*, and *citC*, which code for TCA cycle enzymes. Further, they demonstrated that IsrR decreases the expression of *ccpE*, which codes for a transcriptional activator of *acnA* expression. Fur or IsrR may be required for the expression of the FeS cluster synthesis and FeS protein maturation systems, resulting in decreased holo-AcnA in the Δ*isrR* Δ*fur* strain (59). Although we currently do not know why the AcnA activity in the Δ*isrR* Δ*fur* is lower than that of the WT, it is apparent that *acnA* expression is complex and is regulated by several factors.

We demonstrated that IsrR binds to additional mRNA transcripts that code for enzymes of the TCA cycle, including *sdh, mqo, citM ,* and *citZ*. Activity assays were used to verify that Mqo and Sdh expression was decreased in a Δ*fur* mutant, and this regulation was, in part, relieved by the deletion of *isrR*. As we witnessed with AcnA activity, the activities of Mqo and Sdh are lower in the Δ*isrR* Δ*fur* strain when compared to the WT, suggesting that another factor other than IsrR is regulating expression in the absence of Fur.

The results herein, in combination with previous findings, demonstrate that IsrR represses the expression of mRNA coding the Fe-requiring proteins AcnA, Sdh, GltB2, FdhA, and MiaB (27,50). Coronel-Tellez *et al*. found that an Δ*isrR* mutant had decreased growth when challenged with DIP on solid media supporting the model wherein IsrR functions to spare Fe in *S. aureus* (27). To further support this model, we examined intracellular Fe ion pools. As previously witnessed, a Δ*fur* mutant was more susceptible to killing by streptonigrin, suggesting an increased free Fe pool (7). The deletion of *isrR* lessened this sensitivity of the Δ*fur* mutant but did not return to the levels seen in WT. These data are consistent with a model wherein *isrR* expression promotes an increased Fe ion pool that is not ligated by macromolecules; however, it is currently unknown if this is the result of decreased expression of Fe-requiring proteins or increased Fe uptake or both phenomena. The expression of *isrR* in the Δ*fur* mutant also increased total Fe pools when *S. aureus* was cultured in a rich complex medium under Fe deplete or replete conditions. Production of *S. aureus* siderophore staphyloferrin B (Sbn) requires citrate synthesized from o-phospho-L-serine and glutamate (60). It is tempting to speculate that IsrR decreases TCA cycle function to decrease glutamate anabolism and promote citrate accumulation that can be used for Sbn synthesis. Consistent with this speculation, the introduction of a Δ*isrR* mutation into the Δ*fur* mutant decreased siderophore production. It is currently unknown why the Δ*isrR* strain had increased free Fe and cell-associated Fe compared to the WT strain. The simplest explanation is that the growth media used is unable to fulfill the Fe demands of *S. aureus,* resulting in partial Fur-dependent

derepression of *isrR* transcription in the WT. In the WT, IsrR functions to decrease the expression of iron-requiring enzymes, resulting in an overall decreased Fe load, which does not happen in the Δ*isrR* strain. It is also currently unknown why the Fe-related phenotypes associated with the Δ*isrR* mutation are dominant over the phenotypes associated with the Δ*fur* mutation. The dominant nature of the Δ*isrR* mutation could be explained by IsrR positively influencing the expression of one or more Fe uptake systems. The absence of IsrR results in decreased Fe uptake in the Δ*isrR* Δ*fur* double mutant strain compared to the Δ*fur* strain. Further studies are necessary to parse out the role of IsrR on the regulation of Fe uptake.

So far, IsrR has been shown to regulate ten mRNAs that encompass nitrogen homeostasis (*gltB2, narG, nasD*), fermentation (*fdhA*), tRNA modification (*miaB*), and TCA cycle (*acnA, sdhC, mqo, citM, citZ*) (27,50). IsrR likely functions to repress the expression of these enzymes to spare Fe for use by alternate proteins essential for fitness; however, it is unclear what these proteins are. Fe-S cluster synthesis is essential in *S. aureus*, but the essential Fe-S protein(s) remain elusive (7).

The link between Fe, Fur, and metabolism has been observed across bacteria, including *S. aureus.* This relationship was first explained by the discovery of the Fur-regulated sRNA RyhB in *E. coli* (25,61). RyhB expression results in an Fe-sparing response where non-essential Fe-using proteins involved in processes like the TCA cycle (*acnB, sdh, fumA*), iron storage (*ftnA, bfr*), oxidative stress (*sodB*), respiration (*nuo*), and Fe-S cluster assembly (*isc*) are downregulated in response to Fe limitation (25). RyhB homologs have been found in other enterobacteria such as *Salmonella, Shigella, and Yersinia,* and functional analogs have been described in *Pseudomonas* (PrrF1 and PrrF2) and *B. subtilis* (FsrA) (24,62-65). As Coronel-Tellez *et al*. indicated, it is remarkable that IsrR, although not similar in sequence to these alternate sRNA, functions in a homologous manner to decrease the expression of Fe requiring enzymes and processes (27). Moreover, the expression of these alternate sRNAs is controlled by Fur.

The virulence defects of the *isrR* mutants may suggest a proper Fe sensing and response is required for full host colonization. The importance of Fe homeostasis is highlighted by results showing the colonization defects of strains lacking Fur or IsrR in lung and skin murine models of infection. IsrR was also shown to be required for full lethality of *S. aureus* in a mouse septicemia model (27). A Δ*fur* mutant in the Newman genetic background had increased exoprotein protein, leukotoxin production, hemolysis production, and increased killing of HL-60 cells. However, the Δ*fur* mutant also had decreased survival in a neutrophil-killing assay and in a model of murine pneumonia. Interestingly, the depletion of neutrophils nullified the Δ*fur* mutant's defective lung colonization, suggesting that the Δ*fur* mutant's increased susceptibility to neutrophil killing contributed to its inability to colonize lung tissue (5). This contrasts with our results that did not observe a decrease in pathogenesis with the *fur* mutant. This might be due to the different strains of *S. aureus* used (USA300_LAC and Newman) and the earlier study relying on a higher infection dose. In the skin and soft tissue model of infection, the Δ*isrR* mutant had decreased CFU counts, comparable to levels of the Δ*fur* mutants, but there was no significant decrease in the lesion or necrosis sizes compared to WT. The difference in lesion and necrosis sizes between the Δ*isrR* and the Δ*fur* mutants could be due to a difference in virulence factor regulation. A difference in virulence factor expression could also impact the immune response, affecting the degree of inflammation.

Alternatively, the lower CFU counts of the Δ*isrR* strain might explain the slightly smaller lesion and necrosis sizes compared to WT.

The effect of IsrR on virulence could be indirect and a consequence of metabolite imbalance. Altering metabolic status can impact metabolite pools, which can be sensed by transcriptional regulators that control virulence factor production (51,52). For example, TCA cycle repression could alter GTP and branched-chain amino acid pools (BCAAs), which are sensed by CodY, resulting in altered virulence factor production (66,67). Likewise, IsrR-mediated TCA cycle repression could increase pyruvate titers. Increased pyruvate upregulates virulence factor production in *S. aureus* through complex regulatory networks involving the Agr, Arl, and Sae regulatory systems (68). Further study into the regulatory effects of IsrR should reveal how IsrR contributes to *S. aureus* virulence and will shed light on the cellular response of *S. aureus* to host encountered Fe limitation.

Thanks to high throughput sequencing technologies, hundreds of sRNA candidates have been identified in *S aureus*. Nevertheless, only 50 sRNAs fit the requirements to be *bona fide* trans-acting sRNAs, and around fifteen have been associated with their mRNA targets and biological functions (35). The studies in this manuscript have furthered our understanding of one of these *bona fide* sRNA. The results presented demonstrate that under low Fe growth conditions, Fur derepresses *isrR* transcription. This results in the expression of *isrR,* which modulates the expression of genes that function in the TCA cycle (Fig 10). We also demonstrate that both IsrR and Fur contribute to cellular Fe homeostasis and virulence. Future studies will investigate the mechanisms by which IsrR and Fur alter pathogenesis.

Data Availability Statement

The data underlying this article are available in this article and in its online supplementary material. Strains and plasmids will be made available upon request.

Funding

This work is supported by National Institute of Allergy and Infectious Diseases (NIAID) award [1R01AI139100-01]; National Science Foundation (NSF) award [1750624]; and United State Department of Agriculture MRF project [NE-1028] to J.M.B. D.L. was supported by the Agence Nationale de la Recherche grant [ANR-20-CE12-0021] (MetalAureus). The Bose laboratory is supported by university funds; and National Institutes of Health (NIH) grant [1R21AI156251]. The Parker lab is funded by NIH award [R21AI153646]; and the New Jersey Commission on Cancer Research [COCR22RBG005]. M.J.M. was supported by NIH F31 [AI172352-01A1] and T32 [ES007028] awards.

References

1. Tong, S.Y., Davis, J.S., Eichenberger, E., Holland, T.L. and Fowler, V.G., Jr. (2015) *Staphylococcus aureus* infections: epidemiology, pathophysiology, clinical manifestations, and management. *Clin Microbiol Rev*, **28**, 603-661.
2. De Oliveira, D.M.P., Forde, B.M., Kidd, T.J., Harris, P.N.A., Schembri, M.A., Beatson, S.A., Paterson, D.L. and Walker, M.J. (2020) Antimicrobial Resistance in ESKAPE Pathogens. *Clin Microbiol Rev*, **33**.
3. Mashruwala, A.A., Pang, Y.Y., Rosario-Cruz, Z., Chahal, H.K., Benson, M.A., Mike, L.A., Skaar, E.P., Torres, V.J., Nauseef, W.M. and Boyd, J.M. (2015) Nfu facilitates the maturation of iron-sulfur proteins and participates in virulence in *Staphylococcus aureus*. *Mol Microbiol*, **95**, 383-409.
4. Skaar, E.P., Humayun, M., Bae, T., DeBord, K.L. and Schneewind, O. (2004) Iron-source preference of *Staphylococcus aureus* infections. *Science*, **305**, 1626-1628.
5. Torres, V.J., Attia, A.S., Mason, W.J., Hood, M.I., Corbin, B.D., Beasley, F.C., Anderson, K.L., Stauff, D.L., McDonald, W.H., Zimmerman, L.J. *et al.* (2010) *Staphylococcus aureus* Fur regulates the expression of virulence factors that contribute to the pathogenesis of pneumonia. *Infect Immun*, **78**, 1618-1628.
6. Dale, S.E., Doherty-Kirby, A., Lajoie, G. and Heinrichs, D.E. (2004) Role of siderophore biosynthesis in virulence of Staphylococcus aureus: identification and characterization of genes involved in production of a siderophore. *Infect Immun*, **72**, 29-37.
7. Roberts, C.A., Al-Tameemi, H.M., Mashruwala, A.A., Rosario-Cruz, Z., Chauhan, U., Sause, W.E., Torres, V.J., Belden, W.J. and Boyd, J.M. (2017) The Suf Iron-Sulfur Cluster Biosynthetic System Is Essential in *Staphylococcus aureus*, and Decreased Suf Function Results in Global Metabolic Defects and Reduced Survival in Human Neutrophils. *Infect Immun*, **85**.
8. Murdoch, C.C. and Skaar, E.P. (2022) Nutritional immunity: the battle for nutrient metals at the host-pathogen interface. *Nat Rev Microbiol*, **20**, 657-670.
9. Williams, P. and Griffiths, E. (1992) Bacterial transferrin receptors--structure, function and contribution to virulence. *Med Microbiol Immunol*, **181**, 301-322.
10. Nakashige, T.G., Zhang, B., Krebs, C. and Nolan, E.M. (2015) Human calprotectin is an iron-sequestering host-defense protein. *Nat Chem Biol*, **11**, 765-771.
11. Horsburgh, M.J., Ingham, E. and Foster, S.J. (2001) In *Staphylococcus aureus*, Fur is an interactive regulator with PerR, contributes to virulence, and Is necessary for oxidative stress resistance through positive regulation of catalase and iron homeostasis. *J Bacteriol*, **183**, 468-475.
12. Weiss, G., Ganz, T. and Goodnough, L.T. (2019) Anemia of inflammation. *Blood*, **133**, 40-50.
13. Nairz, M., Theurl, I., Ludwiczek, S., Theurl, M., Mair, S.M., Fritsche, G. and Weiss, G. (2007) The co-ordinated regulation of iron homeostasis in murine macrophages limits the availability of iron for intracellular Salmonella typhimurium. *Cell Microbiol*, **9**, 2126-2140.

14. Silva-Gomes, S., Bouton, C., Silva, T., Santambrogio, P., Rodrigues, P., Appelberg, R. and Gomes, M.S. (2013) Mycobacterium avium infection induces H-ferritin expression in mouse primary macrophages by activating Toll-like receptor 2. *PLoS One*, **8**, e82874.
15. Khan, F.A., Fisher, M.A. and Khakoo, R.A. (2007) Association of hemochromatosis with infectious diseases: expanding spectrum. *Int J Infect Dis*, **11**, 482-487.
16. Sheldon, J.R., Laakso, H.A. and Heinrichs, D.E. (2016) Iron Acquisition Strategies of Bacterial Pathogens. *Microbiol Spectr*, **4**.
17. Hammer, N.D. and Skaar, E.P. (2011) Molecular mechanisms of *Staphylococcus aureus* iron acquisition. *Annual review of microbiology*, **65**, 129-147.
18. Boyd, J.M., Ryan Kaler, K., Esquilin-Lebron, K., Pall, A., Campbell, C.J., Foley, M.E., Rios-Delgado, G., Mustor, E.M., Stephens, T.G., Bovermann, H. *et al.* (2024) Fpa (YlaN) is an iron(II) binding protein that functions to relieve Fur-mediated repression of gene expression in Staphylococcus aureus. *mBio*, e0231024.
19. Friedman, D.B., Stauff, D.L., Pishchany, G., Whitwell, C.W., Torres, V.J. and Skaar, E.P. (2006) *Staphylococcus aureus* redirects central metabolism to increase iron availability. *PLoS Pathog*, **2**, e87.
20. McHugh, J.P., Rodriguez-Quinones, F., Abdul-Tehrani, H., Svistunenko, D.A., Poole, R.K., Cooper, C.E. and Andrews, S.C. (2003) Global iron-dependent gene regulation in *Escherichia coli*. A new mechanism for iron homeostasis. *Journal of Biological Chemistry*, **278**, 29478-29486.
21. Novichkov, P.S., Kazakov, A.E., Ravcheev, D.A., Leyn, S.A., Kovaleva, G.Y., Sutormin, R.A., Kazanov, M.D., Riehl, W., Arkin, A.P., Dubchak, I. *et al.* (2013) RegPrecise 3.0--a resource for genome-scale exploration of transcriptional regulation in bacteria. *BMC genomics*, **14**, 745.
22. Ledala, N., Zhang, B., Seravalli, J., Powers, R. and Somerville, G.A. (2014) Influence of iron and aeration on Staphylococcus aureus growth, metabolism, and transcription. *J Bacteriol*, **196**, 2178-2189.
23. Ganske, A., Busch, L.M., Hentschker, C., Reder, A., Michalik, S., Surmann, K., Volker, U. and Mader, U. (2024) Exploring the targetome of IsrR, an iron-regulated sRNA controlling the synthesis of iron-containing proteins in Staphylococcus aureus. *Front Microbiol*, **15**, 1439352.
24. Gaballa, A., Antelmann, H., Aguilar, C., Khakh, S.K., Song, K.B., Smaldone, G.T. and Helmann, J.D. (2008) The Bacillus subtilis iron-sparing response is mediated by a Fur-regulated small RNA and three small, basic proteins. *Proc Natl Acad Sci U S A*, **105**, 11927-11932.
25. Masse, E. and Gottesman, S. (2002) A small RNA regulates the expression of genes involved in iron metabolism in Escherichia coli. *Proc. Natl. Acad. Sci. USA*, **99**, 4620-4625.
26. Carroll, R.K., Weiss, A., Broach, W.H., Wiemels, R.E., Mogen, A.B., Rice, K.C. and Shaw, L.N. (2016) Genome-wide Annotation, Identification, and Global Transcriptomic Analysis of Regulatory or Small RNA Gene Expression in Staphylococcus aureus. *mBio*, **7**, e01990-01915.

27. Coronel-Tellez, R.H., Pospiech, M., Barrault, M., Liu, W., Bordeau, V., Vasnier, C., Felden, B., Sargueil, B. and Bouloc, P. (2022) sRNA-controlled iron sparing response in Staphylococci. *Nucleic Acids Res*, **50**, 8529-8546.
28. Somerville, G.A., Chaussee, M.S., Morgan, C.I., Fitzgerald, J.R., Dorward, D.W., Reitzer, L.J. and Musser, J.M. (2002) *Staphylococcus aureus* aconitase inactivation unexpectedly inhibits post-exponential-phase growth and enhances stationary-phase survival. *Infect Immun*, **70**, 6373-6382.
29. Kim, G.L., Hooven, T.A., Norambuena, J., Li, B., Boyd, J.M., Yang, J.H. and Parker, D. (2021) Growth and Stress Tolerance Comprise Independent Metabolic Strategies Critical for Staphylococcus aureus Infection. *mBio*, **12**, e0081421.
30. Pang, Y.Y., Schwartz, J., Bloomberg, S., Boyd, J.M., Horswill, A.R. and Nauseef, W.M. (2013) Methionine Sulfoxide Reductases Protect against Oxidative Stress in *Staphylococcus aureus* Encountering Exogenous Oxidants and Human Neutrophils. *J Innate Immun*.
31. Al-Tameemi, H., Beavers, W.N., Norambuena, J., Skaar, E.P. and Boyd, J.M. (2021) Staphylococcus aureus lacking a functional MntABC manganese import system has increased resistance to copper. *Mol Microbiol*, **115**, 554-573.
32. Kreiswirth, B.N., Löfdahl, S., Betley, M.J., O'Reilly, M., Schlievert, P.M., Bergdoll, M.S. and Novick, R.P. (1983) The toxic shock syndrome exotoxin structural gene is not detectably transmitted by a prophage. *Nature*, **305**, 709-712.
33. Novick, R.P. (1991), *Methods in enzymology*. Academic Press, Vol. 204, pp. 587-636.
34. Mashruwala, A.A., Roberts, C.A., Bhatt, S., May, K.L., Carroll, R.K., Shaw, L.N. and Boyd, J.M. (2016) *Staphylococcus aureus* SufT: An essential iron-sulfur cluster assembly factor in cells experiencing a high-demand for lipoic acid. *Mol Microbiol*.
35. Lalaouna, D., Baude, J., Wu, Z., Tomasini, A., Chicher, J., Marzi, S., Vandenesch, F., Romby, P., Caldelari, I. and Moreau, K. (2019) RsaC sRNA modulates the oxidative stress response of Staphylococcus aureus during manganese starvation. *Nucleic Acids Res*, **47**, 9871-9887.
36. Mashruwala, A.A., Bhatt, S., Poudel, S., Boyd, E.S. and Boyd, J.M. (2016) The DUF59 Containing Protein SufT Is Involved in the Maturation of Iron-Sulfur (FeS) Proteins during Conditions of High FeS Cofactor Demand in *Staphylococcus aureus*. *PLoS Genet*, **12**, e1006233.
37. Rosario-Cruz, Z., Chahal, H.K., Mike, L.A., Skaar, E.P. and Boyd, J.M. (2015) Bacillithiol has a role in Fe-S cluster biogenesis in *Staphylococcus aureus*. *Mol Microbiol*, **98**, 218-242.
38. Mashruwala, A.A. and Boyd, J.M. (2017) The *Staphylococcus aureus* SrrAB Regulatory System Modulates Hydrogen Peroxide Resistance Factors, Which Imparts Protection to Aconitase during Aerobic Growth. *PLoS One*, **12**, e0170283.
39. Spencer, M.E. and Guest, J.R. (1973) Isolation and properties of fumarate reductase mutants of *Escherichia coli*. *Journal of Bacteriology*, **114**, 563-570.
40. Schwyn, B. and Neilands, J.B. (1987) Universal chemical assay for the detection and determination of siderophores. *Anal Biochem*, **160**, 47-56.

41. Arora, N.K. and Verma, M. (2017) Modified microplate method for rapid and efficient estimation of siderophore produced by bacteria. *3 Biotech*, **7**, 381.
42. Norambuena, J., Al-Tameemi, H., Bovermann, H., Kim, J., Beavers, W.N., Skaar, E.P., Parker, D. and Boyd, J.M. (2023) Copper ions inhibit pentose phosphate pathway function in Staphylococcus aureus. *PLoS Pathog*, **19**, e1011393.
43. Ridder, M.J., McReynolds, A.K.G., Dai, H., Pritchard, M.T., Markiewicz, M.A. and Bose, J.L. (2022) Kinetic Characterization of the Immune Response to Methicillin-Resistant Staphylococcus aureus Subcutaneous Skin Infection. *Infect Immun*, **90**, e0006522.
44. Boyd, J.M., Esquilín-Lebrón, K., Campbell, C.J., Ryan Kaler, K., Norambuena, J., Foley, M.E., Stephens, T.G., Rios, G., Mereddy, G., Zheng, V. *et al.* (2023) YlaN is an iron(II) binding protein that functions to relieve Fur-mediated repression of gene expression in Staphylococcus aureus. *bioRxiv*.
45. Rauen, U., Springer, A., Weisheit, D., Petrat, F., Korth, H.G., de Groot, H. and Sustmann, R. (2007) Assessment of chelatable mitochondrial iron by using mitochondrion-selective fluorescent iron indicators with different iron-binding affinities. *Chembiochem : a European journal of chemical biology*, **8**, 341-352.
46. Halsey, C.R., Lei, S., Wax, J.K., Lehman, M.K., Nuxoll, A.S., Steinke, L., Sadykov, M., Powers, R. and Fey, P.D. (2017) Amino Acid Catabolism in Staphylococcus aureus and the Function of Carbon Catabolite Repression. *mBio*, **8**.
47. Koch, G., Yepes, A., Forstner, K.U., Wermser, C., Stengel, S.T., Modamio, J., Ohlsen, K., Foster, K.R. and Lopez, D. (2014) Evolution of resistance to a last-resort antibiotic in Staphylococcus aureus via bacterial competition. *Cell*, **158**, 1060-1071.
48. Mann, M., Wright, P.R. and Backofen, R. (2017) IntaRNA 2.0: enhanced and customizable prediction of RNA-RNA interactions. *Nucleic Acids Res*, **45**, W435-W439.
49. Busch, A., Richter, A.S. and Backofen, R. (2008) IntaRNA: efficient prediction of bacterial sRNA targets incorporating target site accessibility and seed regions. *Bioinformatics*, **24**, 2849-2856.
50. Barrault, M., Leclair, E. and Bouloc, P. (2023) Staphylococcal sRNA IsrR down-regulates methylthiotransferase MiaB under iron-deficient conditions. *bioRxiv*.
51. Rudra, P. and Boyd, J.M. (2020) Metabolic control of virulence factor production in Staphylococcus aureus. *Curr Opin Microbiol*, **55**, 81-87.
52. Price, E.E. and Boyd, J.M. (2020) Genetic Regulation of Metal Ion Homeostasis in *Staphylococcus aureus*. *Trends Microbiol*, **28**, 821-831.
53. Kollef, M.H., Shorr, A., Tabak, Y.P., Gupta, V., Liu, L.Z. and Johannes, R.S. (2005) Epidemiology and outcomes of health-care-associated pneumonia: results from a large US database of culture-positive pneumonia. *Chest*, **128**, 3854-3862.
54. Linz, M.S., Mattappallil, A., Finkel, D. and Parker, D. (2023) Clinical Impact of Staphylococcus aureus Skin and Soft Tissue Infections. *Antibiotics (Basel)*, **12**.
55. Neves, J., Haider, T., Gassmann, M. and Muckenthaler, M.U. (2019) Iron Homeostasis in the Lungs-A Balance between Health and Disease. *Pharmaceuticals (Basel)*, **12**.

56. van Dijk, M.C., de Kruijff, R.M. and Hagedoorn, P.L. (2022) The Role of Iron in Staphylococcus aureus Infection and Human Disease: A Metal Tug of War at the Host-Microbe Interface. *Front Cell Dev Biol*, **10**, 857237.
57. Lalaouna, D., Prevost, K., Park, S., Chenard, T., Bouchard, M.P., Caron, M.P., Vanderpool, C.K., Fei, J. and Masse, E. (2021) Binding of the RNA Chaperone Hfq on Target mRNAs Promotes the Small RNA RyhB-Induced Degradation in Escherichia coli. *Noncoding RNA*, **7**.
58. Barrault, M., Chabelskaya, S., Coronel-Tellez, R.H., Toffano-Nioche, C., Jacquet, E. and Bouloc, P. (2024) Staphylococcal aconitase expression during iron deficiency is controlled by an sRNA-driven feedforward loop and moonlighting activity. *Nucleic Acids Res*, **52**, 8241-8253.
59. Esquilin-Lebron, K., Dubrac, S., Barras, F. and Boyd, J.M. (2021) Bacterial Approaches for Assembling Iron-Sulfur Proteins. *mBio*, **12**, e0242521.
60. Cheung, J., Murphy, M.E. and Heinrichs, D.E. (2012) Discovery of an iron-regulated citrate synthase in Staphylococcus aureus. *Chemistry & biology*, **19**, 1568-1578.
61. Wassarman, K.M., Repoila, F., Rosenow, C., Storz, G. and Gottesman, S. (2001) Identification of novel small RNAs using comparative genomics and microarrays. *Genes Dev*, **15**, 1637-1651.
62. Wilderman, P.J., Sowa, N.A., FitzGerald, D.J., FitzGerald, P.C., Gottesman, S., Ochsner, U.A. and Vasil, M.L. (2004) Identification of tandem duplicate regulatory small RNAs in Pseudomonas aeruginosa involved in iron homeostasis. *Proc Natl Acad Sci U S A*, **101**, 9792-9797.
63. Deng, Z., Meng, X., Su, S., Liu, Z., Ji, X., Zhang, Y., Zhao, X., Wang, X., Yang, R. and Han, Y. (2012) Two sRNA RyhB homologs from Yersinia pestis biovar microtus expressed in vivo have differential Hfq-dependent stability. *Res Microbiol*, **163**, 413-418.
64. Murphy, E.R. and Payne, S.M. (2007) RyhB, an iron-responsive small RNA molecule, regulates Shigella dysenteriae virulence. *Infect Immun*, **75**, 3470-3477.
65. Kim, J.N. and Kwon, Y.M. (2013) Identification of target transcripts regulated by small RNA RyhB homologs in Salmonella: RyhB-2 regulates motility phenotype. *Microbiol Res*, **168**, 621-629.
66. Brinsmade, S.R. (2017) CodY, a master integrator of metabolism and virulence in Gram-positive bacteria. *Curr Genet*, **63**, 417-425.
67. Mlynek, K.D., Sause, W.E., Moormeier, D.E., Sadykov, M.R., Hill, K.R., Torres, V.J., Bayles, K.W. and Brinsmade, S.R. (2018) Nutritional Regulation of the Sae Two-Component System by CodY in Staphylococcus aureus. *J Bacteriol*, **200**.
68. Harper, L., Balasubramanian, D., Ohneck, E.A., Sause, W.E., Chapman, J., Mejia-Sosa, B., Lhakhang, T., Heguy, A., Tsirigos, A., Ueberheide, B. *et al.* (2018) Staphylococcus aureus Responds to the Central Metabolite Pyruvate To Regulate Virulence. *mBio*, **9**.
69. Price, E.E., Rudra, P., Norambuena, J., Roman-Rodriguez, F. and Boyd, J.M. (2021) Tools, Strains, and Strategies To Effectively Conduct Anaerobic and Aerobic Transcriptional Reporter Screens and Assays in *Staphylococcus aureus*. *Appl Environ Microbiol*, **87**, e0110821.

70. Bose, J.L., Fey, P.D. and Bayles, K.W. (2013) Genetic tools to enhance the study of gene function and regulation in *Staphylococcus aureus*. *Appl Environ Microbiol*, **79**, 2218-2224.
71. Forsyth, R.A., Haselbeck, R.J., Ohlsen, K.L., Yamamoto, R.T., Xu, H., Trawick, J.D., Wall, D., Wang, L., Brown-Driver, V., Froelich, J.M. *et al.* (2002) A genome-wide strategy for the identification of essential genes in *Staphylococcus aureus*. *Mol Microbiol*, **43**, 1387-1400.
72. Bubeck Wardenburg, J., Williams, W.A. and Missiakas, D. (2006) Host defenses against *Staphylococcus aureus* infection require recognition of bacterial lipoproteins. *Proc Natl Acad Sci U S A*, **103**, 13831-13836.
73. Luong, T.T. and Lee, C.Y. (2007) Improved single-copy integration vectors for *Staphylococcus aureus*. *J Microbiol Methods*, **70**, 186-190.

Tables

Table 1. *Staphylococcus aureus* USA300_LAC strains used in this study.

Strain name	Genotype	Reference
JMB1100	USA300_LAC wild type (WT)	A. Horswill
JMB10842	Δ*fur::tetM*	(34)
JMB10495	Δ*fur::tetM isrR**	This study
JMB11112	Δ*fur::tetM* SAUSA300_1309::Tn	This study
JMB11113	Δ*fur::tetM isrR** SAUSA300_1309::Tn	This study
JMB11292	Δ*isrR*	This study
JMB11293	Δ*fur::tetM* Δ*isrR*	This study
JMB1886	*geh*::pLL39	(69)
JMB11803	*acnA::Tn*	(37)
JMB7868	Δ*acnA::tetM*	(28)
JMB14375	*sdhA::Tn*	This study
JMB11804	*acnA::Tn* Δ*fur::tetM*	This study
JMB11805	*acnA::Tn* Δ*isrR*	This study
JMB11806	*acnA::Tn* Δ*fur::tetM* Δ*isrR*	This study
JMB11448	SAUSA300_1456::Tn *geh*::pLL39	This study
JMB11449	$fur_{E11Stop}$ SAUSA300_1456::Tn *geh::*pLL39	This study
JMB11395	Δ*isrR* SAUSA300_1456::Tn *geh::*pLL39	This study
JMB11392	$fur_{E11Stop}$ Δ*isrR* SAUSA300_1456::Tn *geh::*pLL39	This study
JMB11393	$fur_{E11Stop}$ Δ*isrR* SAUSA300_1456::Tn *geh::*pLL39_*isrR*	This study
JMB13983	$fur_{E11Stop}$ Δ*isrR* SAUSA300_1456::Tn *geh::*pLL39_*isrR_C1*	This study
JMB13984	$fur_{E11Stop}$ Δ*isrR* SAUSA300_1456::Tn *geh::*pLL39_*isrR_C2*	This study
JMB13985	$fur_{E11Stop}$ Δ*isrR* SAUSA300_1456::Tn *geh::*pLL39_*isrR_C1_C2*	This study
JMB14888	$fur_{E11Stop}$ Δ*isrR* SAUSA300_1456::Tn *geh::*pLL39_*isrR_C2a*	This study

Table 2. Plasmids used in this study

Name	Function	Reference
pJB38	Mutant generation	(70)
pJB38_Δ*isrR*	Δ*isrR* mutant generation	This study
pEPSA5	Inducible expression complementation	(71)
pEPSA5_*isrR*	Inducible expression *isrR*	This study
pEPSA5_as_*isrR*	Inducible expression *isrR* antisense	This study
pEPSA5_trunk_*isrR*	Inducible expression truncated *isrR*	This study
pEPSA5_*isrR**	Inducible expression *isrR**	This study
pEPSA5_*acnA*	Non-native promoter expression	This study
pOS-1-p*lgt*	Genetic complementation *lgt* promoter	(72)
pOS-1-p*lgt_fur*	Genetic complementation *lgt* promoter	(5)
pOS_p*isrR_gfp*	*isrR* transcriptional reporter	This study
pOS_p*isrR*_gfp*	*isrR** transcriptional reporter	This study
pLL39	Genetic complementation	(73)
pLL39_*isrR*	Native promoter complementation	This study
pLL39_*isrR_C1*	Native promoter complementation	This study
pLL39_*isrR_C2*	Native promoter complementation	This study
pLL39_*isrR_C1_C2*	Native promoter complementation	This study
pLL39_*isrR_C2a*	Native promoter complementation	This study
pOS_p*lgt_acnA_gfp*	*acnA* translational reporter	This study
pOS_p*lgt_acnA1_gfp*	Mutated *acnA* translational reporter	This study
pOS_p*lgt_acnA2_gfp*	Mutated *acnA* translational reporter	This study

Figures and Figure Legends

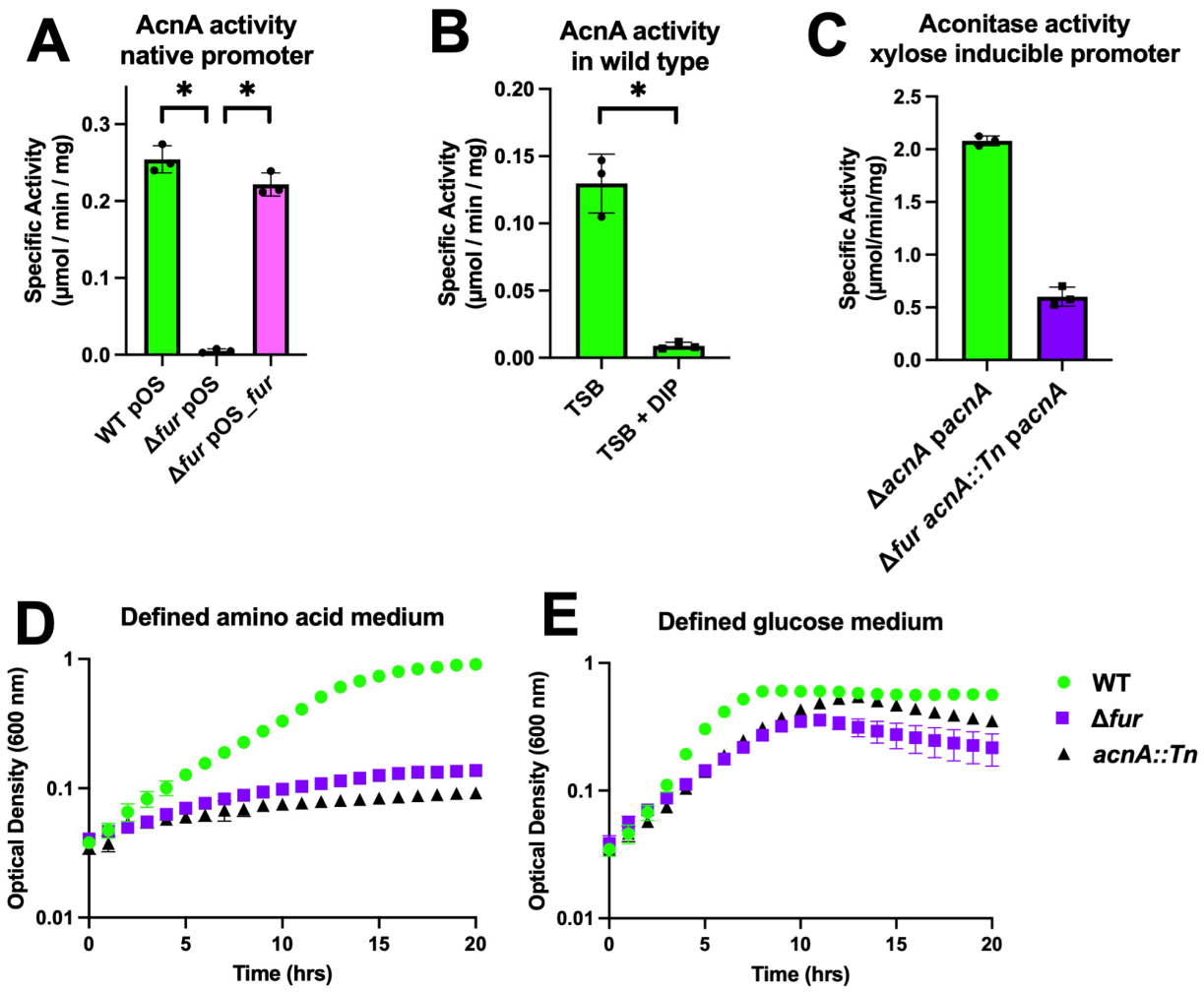

Figure 1. A *S. aureus* Δ*fur* mutant has decreased aconitase expression. **Panel A.** Aconitase activity was quantified in cell free lysates harvested from the wild type (WT) (JMB1100) and Δ*fur::tetM* (JMB10842) strains carrying pOS-1-p*lgt* or pOS-1-p*lgt_fur* after culture in TSB-Cm medium. **Panel B.** Aconitase activity was quantified in cell-free lysates from the WT after culture in TSB +/- 250 µM 2,2' dipyridyl (DIP). **Panel C.** Aconitase activity was quantified in cell-free lysates harvested from the *acnA::Tn* (JMB11803) and Δ*fur::tetM acnA::Tn* (JMB11804) strains with pEPSA5_*acnA* after culture in TSB-Cm medium supplemented with 0.25% xylose. **Panel D.** Culture optical densities (A_{600}) were monitored for the WT, Δ*fur::tetM,* and *acnA::Tn* strains in a liquid-defined medium containing amino acids as the sole carbon and energy sources. **Panel E.** Culture optical densities (A_{600}) of the WT, Δ*fur::tetM,* and *acnA::Tn* strains were monitored in a liquid-defined medium containing amino acids supplemented with 10 mM glucose. The data shown represent the average of biological triplicates with standard deviations shown. Error bars are shown for all data but in some cases (Panels D and E) are smaller than the symbols used. Student's two-tailed t-tests were performed on the data and * represents a p-value of <0.05.

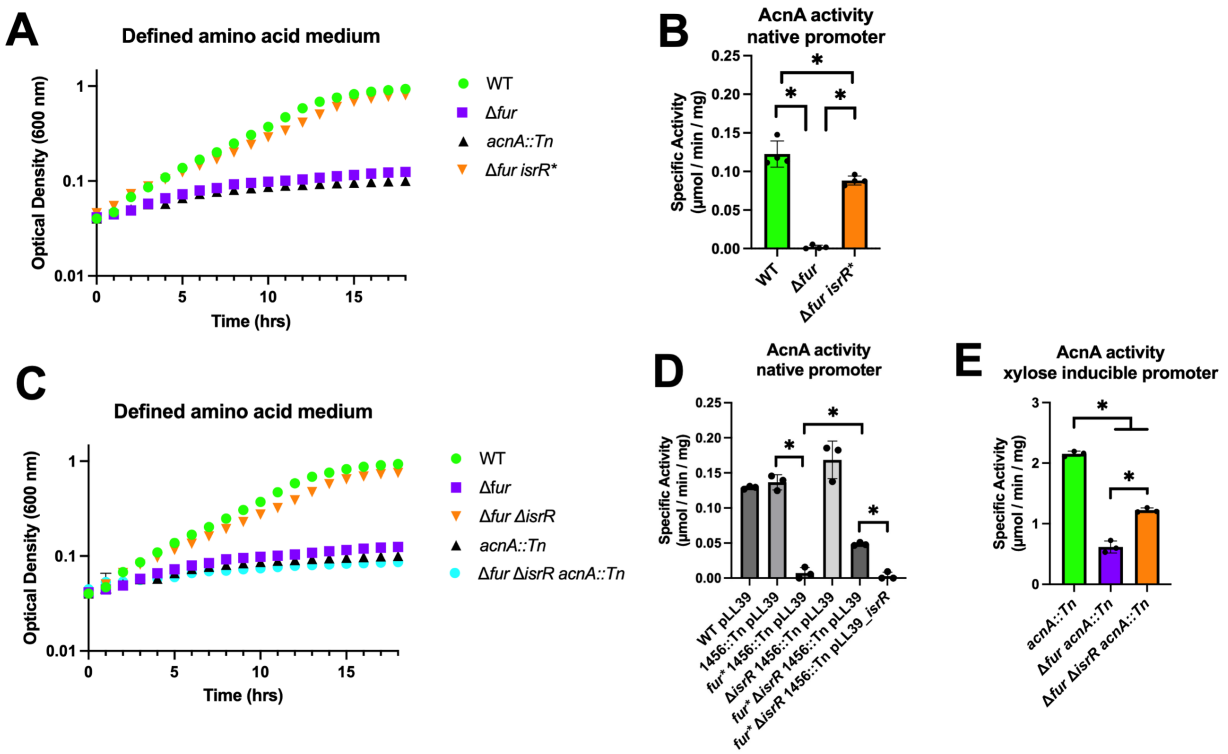

Figure 2. A null mutation in *isrR* suppresses the amino acid growth defect and increases aconitase (AcnA) activity of a Δ*fur* mutant. **Panel A.** Culture optical densities (A_{600}) of the wild type (WT) (JMB1100), Δ*fur::tetM* (JMB10842), Δ*fur::tetM isrR** (JMB10495), and *acnA::Tn* (JMB11803) strains were monitored when cultured on defined medium containing amino acids as carbon and energy sources. **Panel B.** Aconitase activity was quantified in cell free lysates harvested from the WT, Δ*fur::tetM,* and Δ*fur::tetM isrR** strains after culture in TSB medium. **Panel C.** Culture optical densities (A_{600}) of the WT, *acnA::Tn,* Δ*fur::tetM,* Δ*fur::tetM* Δ*isrR* (JMB11293), and Δ*fur::tetM* Δ*isrR acnA::Tn* (JMB11806) strains were monitored in liquid defined medium containing amino acids as carbon and energy sources. **Panel D.** Aconitase activity was quantified in cell free lysates harvested from the WT with pLL39 (JMB1886), SAUSA300_1456::Tn (*1456::Tn*) pLL39 (JMB11448), *fur* 1456::Tn* pLL39 (JMB11449), Δ*isrR 1456::Tn* pLL39 (JMB11395), *fur** Δ*isrR 1456::Tn* pLL39 (JMB11392), and *fur** Δ*isrR 1456::Tn* pLL39_*isrR* (JMB11393) strains after culture in TSB medium. **E.** Aconitase activity was quantified in cell-free lysates harvested from the *acnA::Tn,* Δ*fur::tetM acnA::Tn* (JMB11804), and Δ*fur::tetM* Δ*isrR acnA::Tn* strains containing pEPSA5_*acnA* after culture in TSB-Cm medium supplemented with 0.25% xylose. The data shown represent the average of biological triplicates with standard deviations shown. Error bars are shown for all data but in some cases (Panels D and E) are smaller than the symbols used. Student's two-tailed t-tests were performed on the data and * represents a p-value of <0.05.

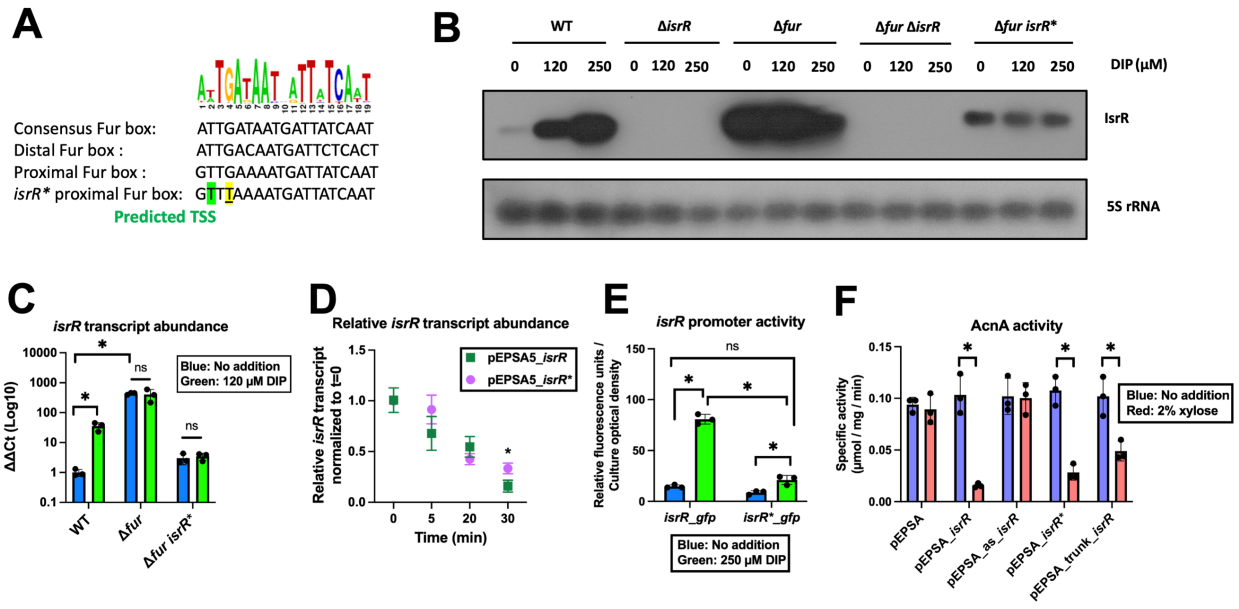

Figure 3. The *isrR** mutation suppresses the phenotypes of the Δ*fur* mutant by decreasing *isrR* transcription. **Panel A.** Top, predicted consensus Fur box sequence as determined by RegPrecise, and bottom, consensus Staphylococcal Fur box, *isrR* distal Fur box, *isrR* proximal Fur box, and proximal Fur box in the *isrR** strains with change highlighted in yellow and underlined. The transcriptional start site, as determined by 5' RACE analysis, is highlighted in green (27). **Panel B.** Northern blot analysis of IsrR transcripts using total RNA isolated from wild type (WT)(JMB1100), Δ*isrR* (JMB11292), Δ*fur* (JMB10842), Δ*fur* Δ*isrR* (JMB11293), and Δ*fur isrR** (JMB10495) strains after culture in TSB media containing 0, 120, or 500 μM 2,2' dipyridyl (DIP). **Panel C.** IsrR transcript abundance in the WT, Δ*fur,* and Δ*fur isrR** strains after culture in liquid TSB media supplemented with or without 120 μM DIP. Transcript abundance was determined by quantitative PCR. **Panel D.** Quantification of transcripts corresponding to *isrR* after the Δ*fur::tetM* Δ*isrR* strain carrying either pEPSA5_*isrR* or pEPSA5_*isrR** were cultured in TSB medium containing 2% xylose and subsequently rifampicin was added (t=0) to inhibit transcription. Transcript abundances were normalized to t=0. **Panel E.** Relative fluorescence of the WT strain containing the pOS_p*isrR_gfp* or pOS_p*isrR*_gfp* transcriptional reporter after culture in TSB-Cm with or without 250 μM DIP. **Panel F.** Aconitase activity in cell-free lysates from the WT strain carrying pEPSA5, pEPSA5_*isrR*, pEPSA5_as_*isrR,* pEPSA5_*isrR**, and pEPSA5_trunk_*isrR* after culture in TSB-Cm with or without 2% xylose. Panels B contains representative Northern blots. The data displayed in panels C-F represent the average of biological triplicates with standard deviations shown. Student's two-tailed t-tests were performed on the data and * represents a p-value of <0.05.

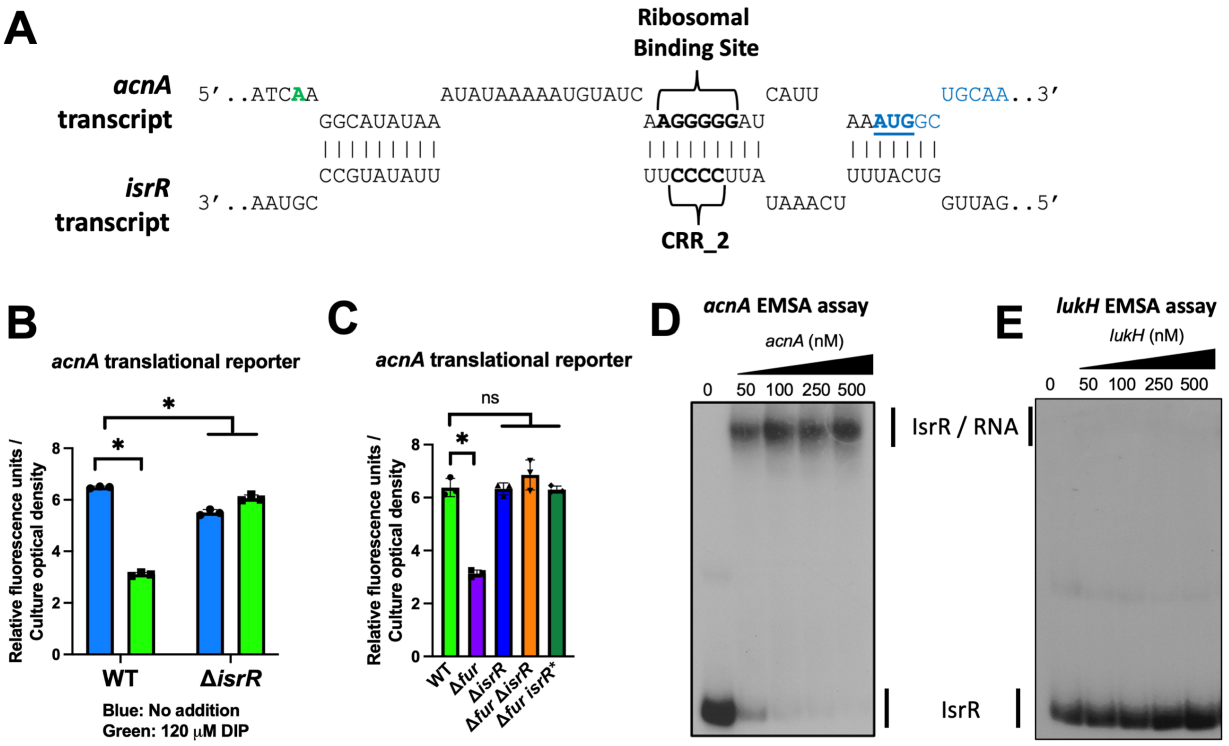

Figure 4. IsrR directly influences *acnA* translation. **Panel A.** IntaRNA predicted interaction between IsrR and *acnA* mRNA transcript. Predicted interaction includes the *acnA* Shine Dalgarno sequence (ribosomal binding site) and the second cytosine-rich region (CRR_2) of IsrR. The *acnA* mRNA AUG start codon is underlined and bolded, and the AcnA coding sequence is in blue. The base indicating the predicted transcriptional start site from Figure S7 is in green. **Panel B.** Relative fluorescence of the wild type (WT) (JMB1100) and Δ*isrR* (JMB11292) strains containing the pOS_p*lgt_acnA_gfp* translational reporter after culture in TSB-Cm media with or without 120 μM DIP. **Panel C.** Relative fluorescence of the WT, Δ*isrR,* Δ*fur::tetM* (JMB10842), Δ*fur::tetM* Δ*isrR* (JMB11293), and Δ*fur::tetM isrR** (JMB10495) strains containing the pOS_p*lgt_acnA_gfp* translational reporter after culture in TSB-Cm medium. **Panel D.** Electrophoretic mobility shift assay (EMSA) using 20,000 cpm of radiolabeled IsrR and 0-500 μM of the *acnA* transcript. **Panel E.** EMSA using 20,000 cpm of radiolabeled IsrR and 0-500 μM of the *lukH* transcript. The data in panels B and C represent the average of biological triplicates with standard deviations shown. Student's two-tailed t-tests were performed on the data and * represents a p-value of <0.05. Pictures of representative EMSA assays (n=2) are displayed in panels D and E.

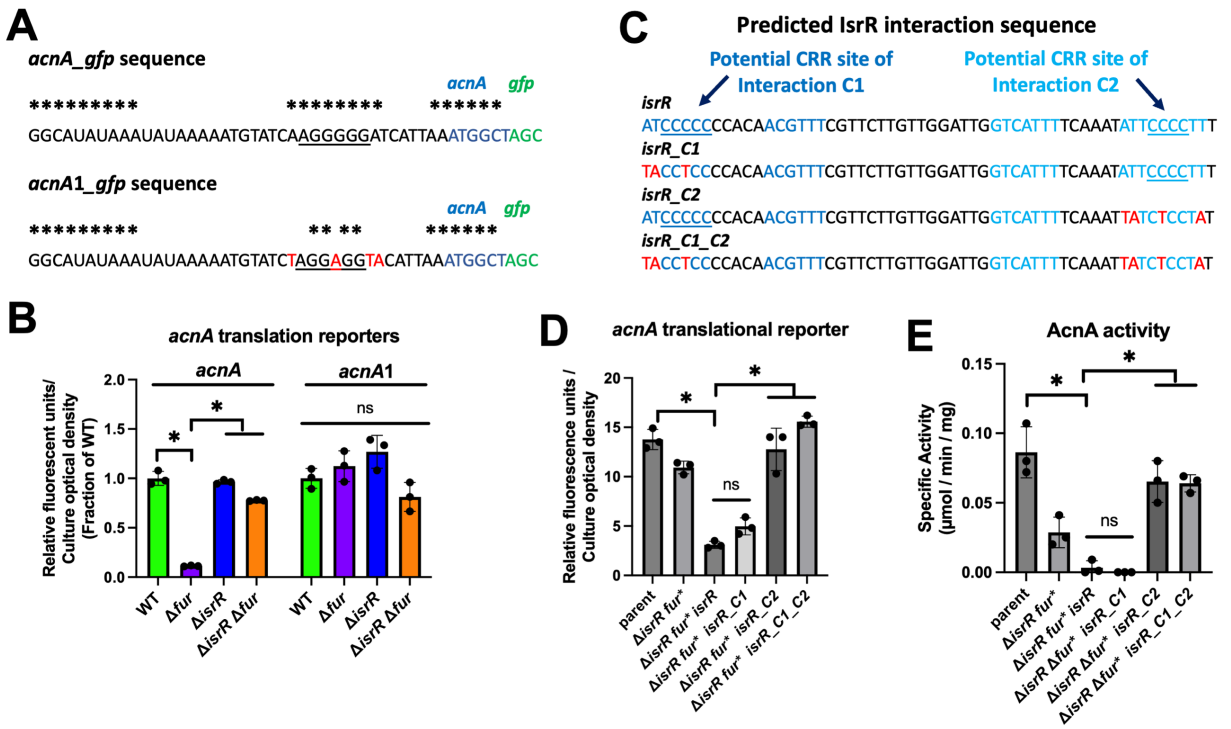

Figure 5. Interactions between the *acnA* Shine Dalgarno sequence nucleotides and a cytosine-rich region (CRR) of IsrR may influence IsrR-mediated *acnA* translational repression. **Panel A.** Partial sequences of the *acnA_gfp* and *acnA1_gfp* translational reporters. Black indicates *acnA* 5' untranslated region (UTR), the *acnA* Shine Dalgarno sequence is underlined, blue indicates the first two codons of *acnA*, green indicates the start of the *gfp* sequence, and an asterisk above the nucleotide denotes that they are predicted to interact with IsrR. Red nucleotides in the lower sequence indicate substitutions in the *acnA1_gfp* translational reporter. **Panel B.** Relative fluorescence of the wild type (WT) (JMB1100), Δ*fur::tetM* (JMB10842), Δ*isrR* (JMB11292), and Δ*fur::tetM* Δ*isrR* (JMB11293) strains containing the *acnA_gfp* or *acnA1_gfp* translational reporters cultured in TSB-Cm medium. **Panel C.** Portions of IsrR and IsrR variant sequences (*isrR_C1, isrR_C2, isrR_C1_C2*) that are predicted to interact with *acnA* mRNA. Blue indicates nucleotides involved in the predicted interaction, including cytosine-rich regions one (CRR_1; dark blue) and two (CCR_2; light blue). Underlined nucleotides indicate the IsrR C-rich regions. Red indicates the nucleotide substitutions in the *isrR* variants. **Panel D.** Relative fluorescence of the *1456::Tn* pLL39 (JMB11448) (parent), *fur** Δ*isrR 1456::Tn* pLL39 (JMB11392), *fur** Δ*isrR 1456::Tn* pLL39_*isrR* (JMB11393), *fur** Δ*isrR 1456::Tn* pLL39_*isrR_C1* (JMB13983), *fur** Δ*isrR 1456::Tn* pLL39_*isrR_C2* (JMB13984), and *fur** Δ*isrR 1456::Tn* pLL39_*isrR_C1_C2* (JMB14314) containing the pOS_p*lgt_acnA_gfp* translational reporter. **Panel E.** Aconitase activity in cell free lysates harvested from the strains in panel D after culture in TSB medium. The data in panels B, D, and E represent the average of biological triplicates with standard deviations shown. Student's two-tailed t-tests were performed on the data, and * represents a p-value of <0.05.

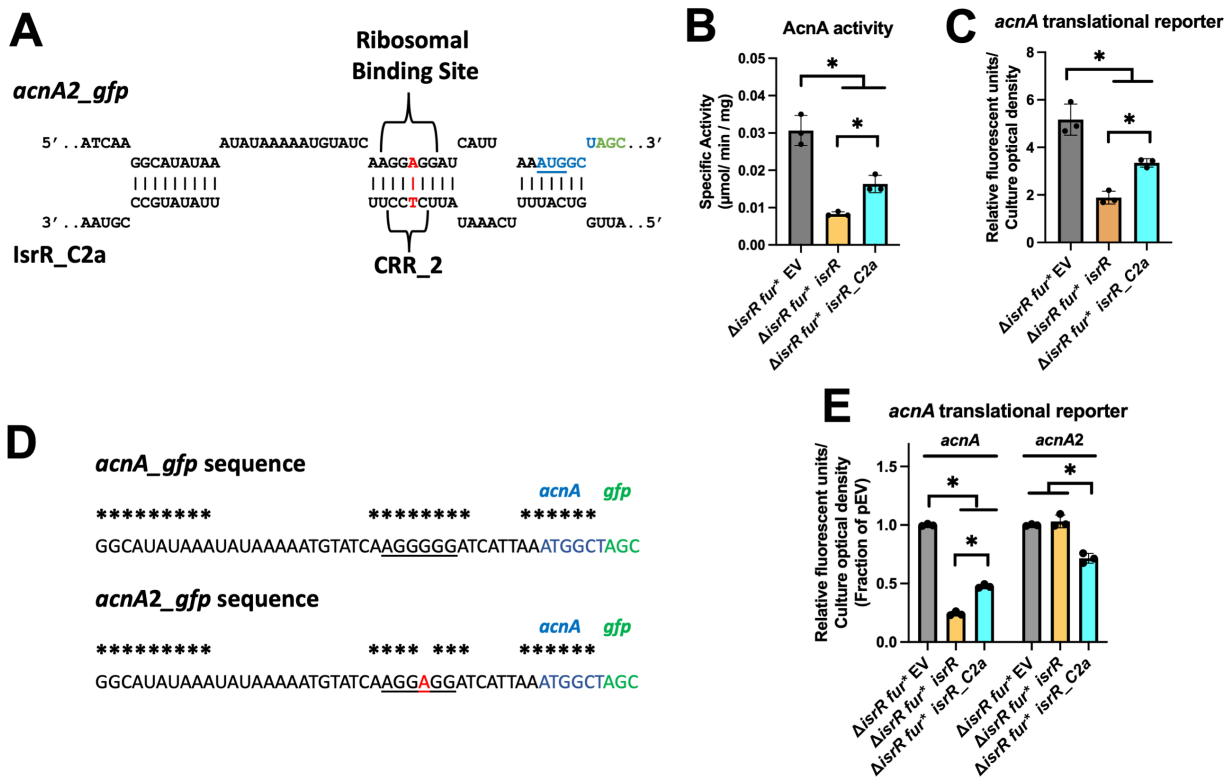

Figure 6. Compensatory interactions between IsrR CRR_2 and the *acnA* ribosomal binding site reestablish IsrR-mediated control of aconitase expression. **Panel A.** IntaRNA predicted interaction between the pOS_p*lgt_acnA2_gfp* and IsrR_C2a sequences. The mutated bases for both *acnA2_gfp* and IsrR_C2a are in red, blue indicates the first two codons of *acnA,* the *acnA* mRNA AUG start codon is underlined, and green indicates the first codon of *gfp.* **Panel B.** Aconitase activity in cell-free lysates harvested from *fur** Δ*isrR 1456::Tn* pLL39 (JMB11392), *fur** Δ*isrR 1456::Tn* pLL39_*isrR* (JMB11393), and *fur** Δ*isrR 1456::Tn* pLL39_*isrR_C2a* (14888) after culture in TSB medium. **Panel C.** Relative fluorescence of the strains in panel B containing the pOS_p*lgt_acnA_gfp* translational reporter after culture in TSB-Cm medium. **Panel D.** Partial sequences of the *acnA_gfp* and *acnA2_gfp* translational reporters. Black indicates *acnA* 5' untranslated region (UTR), the *acnA* Shine Dalgarno sequence is underlined, blue indicates the first two codons of *acnA*, green indicates the start of the *gfp* sequence, and an asterisk above the nucleotide denotes that they are predicted to interact with IsrR. The red nucleotide in the lower sequence indicates the substitution in the *acnA2_gfp* translational reporter. **Panel E.** Relative fluorescence of the strains in panel B containing the pOS_p*lgt_acnA_gfp* or pOS_p*lgt_acnA2_gfp* translational reporters after culture in TSB-Cm medium. The data displayed in panels B, C, and E represent the average of biological triplicates with standard deviations shown. Student's two-tailed t-tests were performed on the data, and * represents a p-value of <0.05.

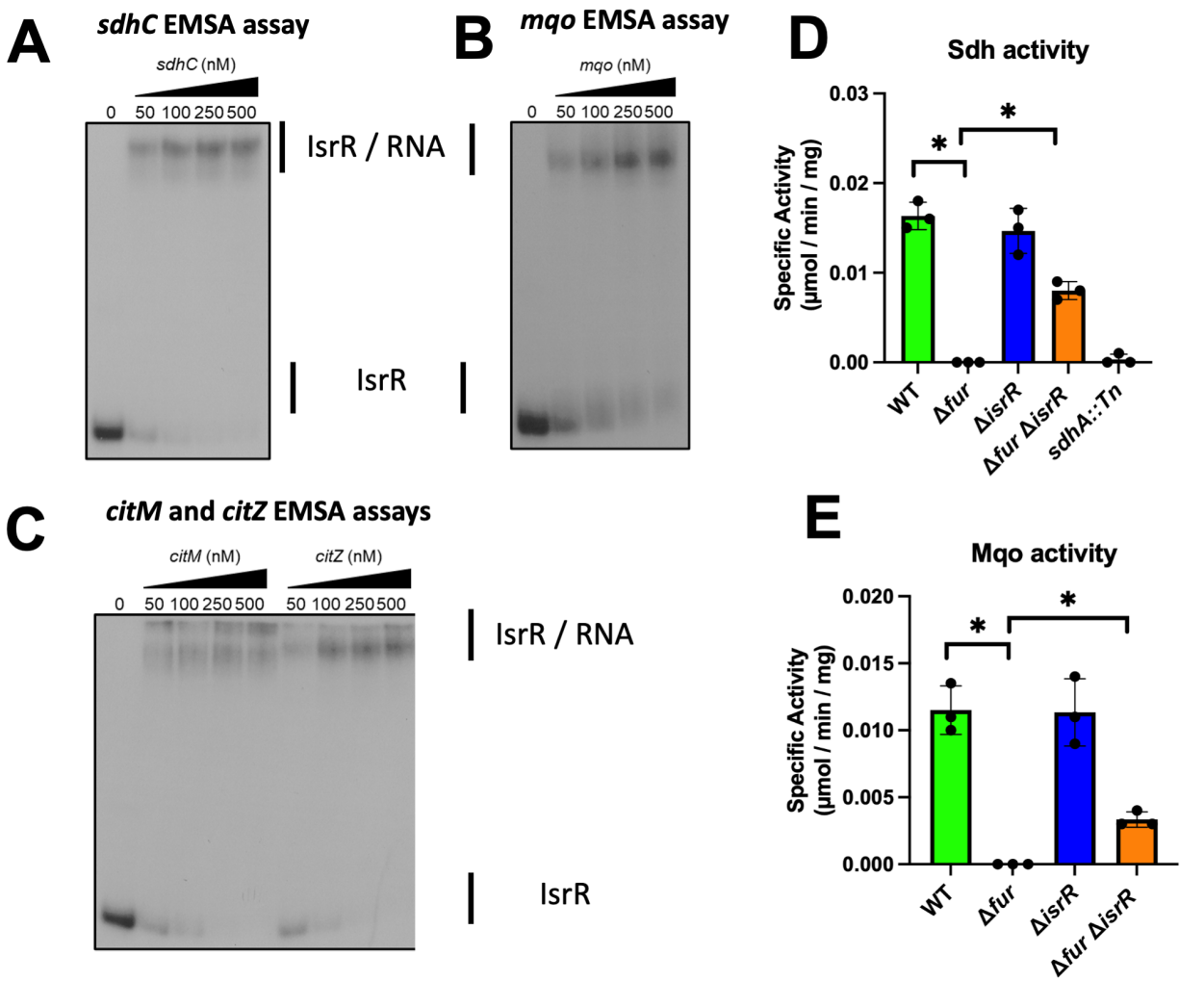

Figure 7. IsrR interacts with TCA cycle mRNAs and affects expression. **Panel A.** Electrophoretic mobility shift assay (EMSA) using 20,000 cpm of radiolabeled IsrR and 0-500 nM of the *sdhC* transcript. **Panel B.** EMSA using 20,000 cpm of radiolabeled IsrR and 0-500 nM of the *mqo* transcript. **Panel C.** EMSA using 20,000 cpm of radiolabeled IsrR and 0-500 nM of the *citZ* or *citM* transcripts. **Panel D.** Activity of succinate dehydrogenase (Sdh) was quantified in cell-free lysates generated from the wild type (WT) (JMB1100), Δ*fur::tetM* (JMB10842), Δ*isrR* (JMB11292), Δ*fur::tetM* Δ*isrR* (JMB11293), and *sdhA::Tn* (JMB14375) strains after culture in TSB medium. **Panel E.** Activity of malate quinone oxidoreductase (Mqo) in cell-free lysates generated from the WT, Δ*fur::tetM,* Δ*isrR,* and Δ*fur::tetM* Δ*isrR* strains. Pictures of representative EMSA assays (n=2) are displayed in panels A-C. The data displayed in panels D and E represent the average of biological triplicates with standard deviations shown. Student's two-tailed t-tests were performed on the data, and * represents a p-value of <0.05.

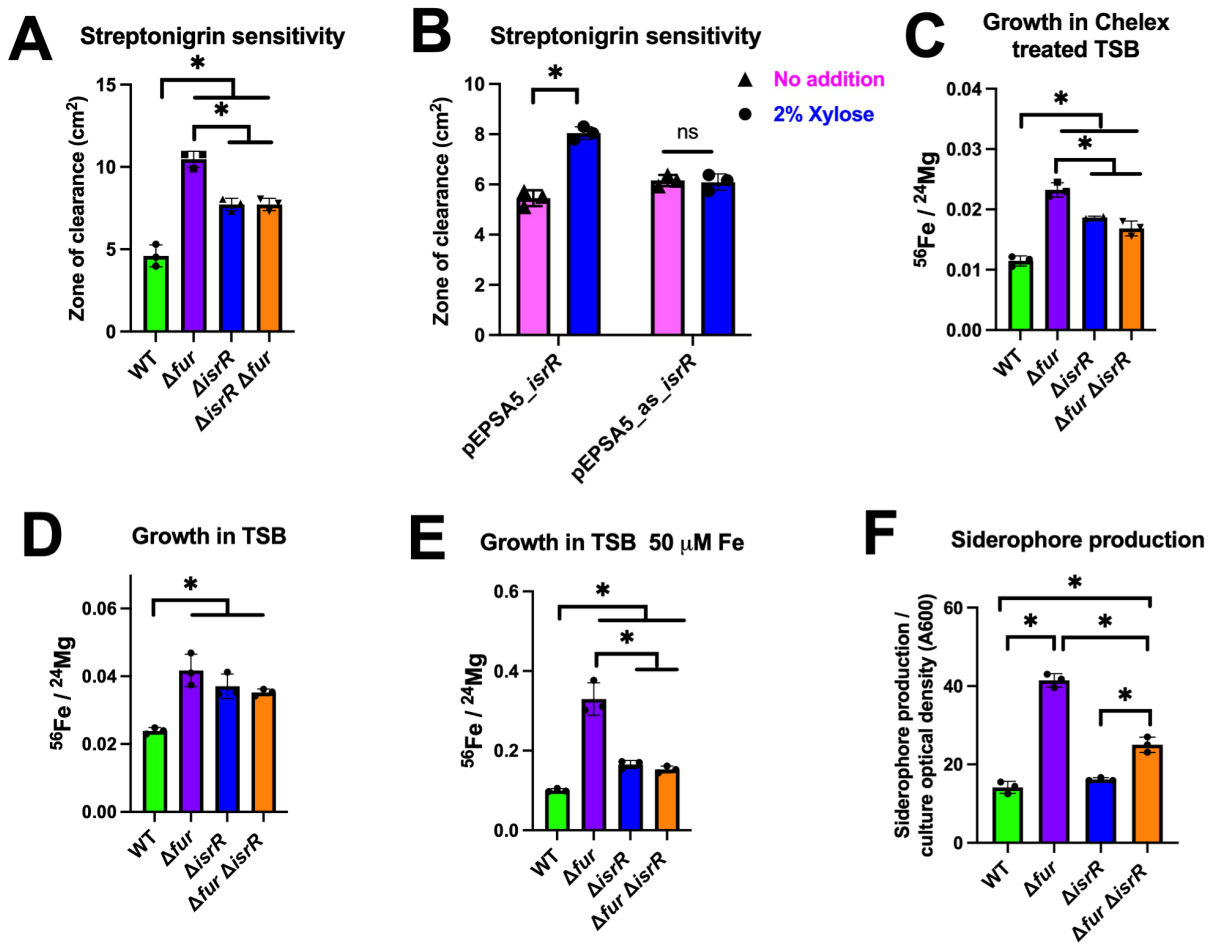

Figure 8. IsrR impacts iron homeostasis. **Panel A.** The wild type (WT)(JMB1100), Δ*fur::tetM* (JMB10842), Δ*isrR* (JMB11292), and Δ*fur::tetM* Δ*isrR* (JMB11293) strains were plated as top agar overlays on solid TSA, followed by spotting 2.5 µg streptonigrin. **Panel B.** The WT strain containing pEPSA5_*isrR* or pEPSA_as_*isrR* were plated as top agar overlays on solid TSA-Cm with or without 2% xylose, followed by spotting 2.5 µg streptonigrin. For Panels A and B, the zones of clearance resulting from streptonigrin growth inhibition was quantified. **Panels C, D, and E.** The ratio of ^{56}Fe and ^{24}Mg abundances were quantified in whole cells using ICP-MS after culture in Chelex-treated TSB (Panel C), TSB (Panel D), or TSB supplemented with 50 µM Fe (Panel E). The ratio of ^{56}Fe / ^{24}Mg is displayed for WT, Δ*fur::tetM,* Δ*isrR,* and Δ*fur::tetM* Δ*isrR* strains. **Panel F**. Siderophore production from spent culture supernatants from the WT, Δ*fur::tetM,* Δ*isrR,* and Δ*fur::tetM* Δ*isrR* strains was quantified. The data displayed represent the average of biological triplicates with standard deviations shown. Student's two-tailed t-tests were performed on the data, and * represents a p-value of <0.05.

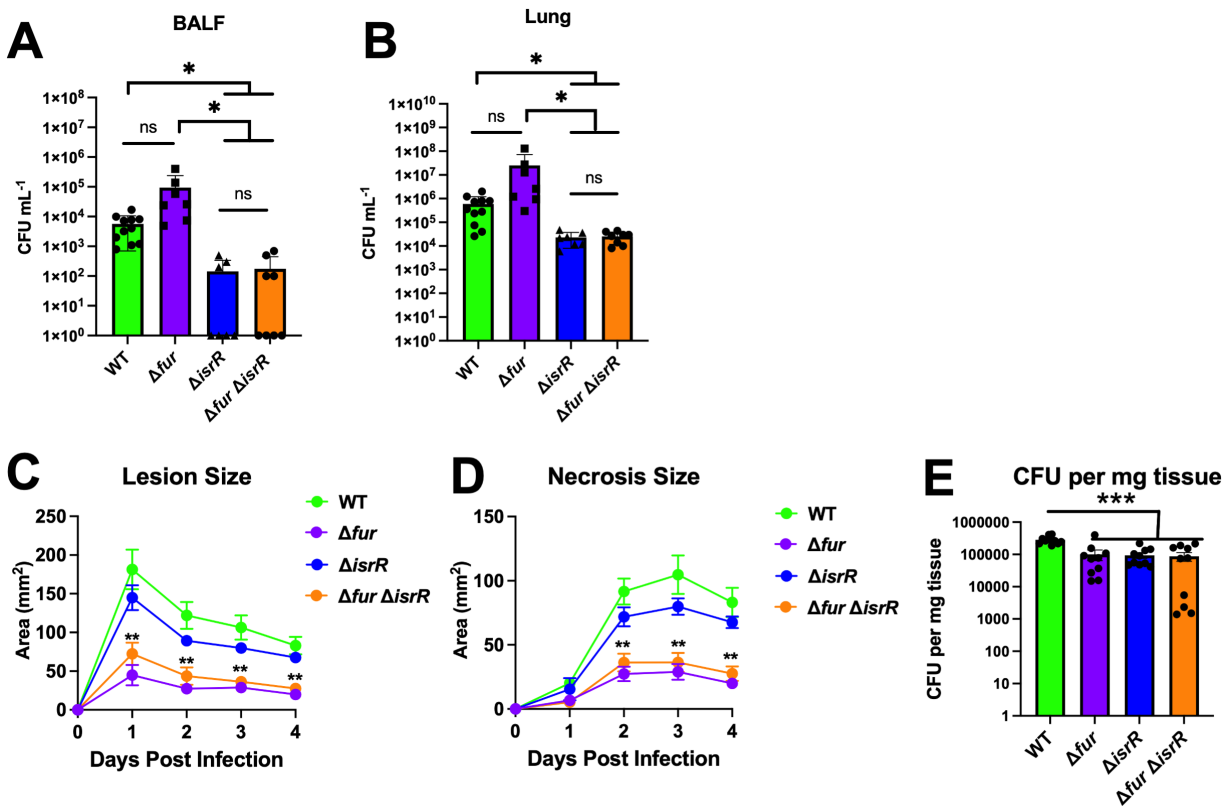

Figure 9. IsrR and Fur are important for tissue damage and colonization during infection. **Panels A** and **B.** The wild type (WT)(JMB1100), Δ*fur::tetM* (JMB10842), Δ*isrR* (JMB11292), and Δ*fur::tetM* Δ*isrR* (JMB11293) strains were tested in a model of acute pneumonia infection. Data represent bacterial counts 24 hours after intranasal infection in bronchoalveolar lavage fluid (Panel A) and lung tissue (Panel B). **Panels C and D**, the wild type (WT), Δ*fur::tetM,* Δ*isrR,* and Δ*fur::tetM* Δ*isrR* strains were injected subcutaneously into C57BL/6J mice and total lesion size (Panel C) and necrosis size (Panel D) were monitored over time. **Panel E**. Local bacterial titers were quantified four days post-infection. For Panels C and D, the data is a representative experiment with n=10, and error bars represent the SEM. Each dot is an individual animal for panels A, B, and E, and the bar or line represents the mean. Error bars represent the SEM and may be smaller than symbols. * , **, and *** indicates $p<0.05$, $p<0.01$, and $p<0.001$, respectively, by Mann-Whitney test.

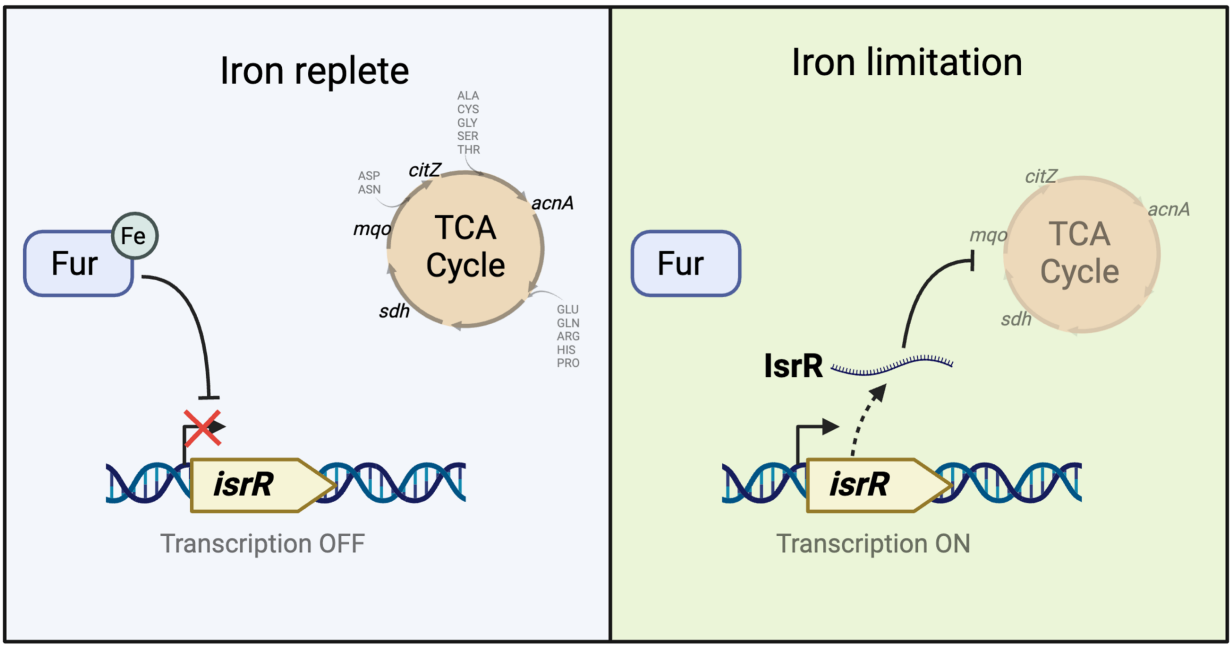

Figure 10. Model for IsrR-dependent regulation of TCA cycle expression. Growth in iron ion replete conditions results in metalation of Fur and transcriptional repression of *isrR*, which produces a non-coding small regulatory RNA. Upon iron limitation, Fur is demetallated, and *isrR* is expressed. IsrR forms complexes with the *acnA*, *sdh*, *citM*, and *citZ* mRNA transcripts resulting in decreased expression and decreased carbon flux through the TCA cycle. Decreased expression of TCA cycle enzymes results in an inability to grow using amino acids for carbon and energy. This figure was created using Biorender.